STATE OF OREGON
DEPARTMENT OF GEOLOGY AND MINERAL INDUSTRIES
910 State Office Building
Portland, Oregon 97201

OPEN-FILE REPORT O-86-16

HYDROTHERMAL SULFIDES, BRECCIAS, AND GREENSTONES FROM THE GORDA DEPRESSION

By Roger Hart, Douglas Pyle, and James Robbins,
College of Oceanography, Oregon State University,
Corvallis, Oregon 97331

Final Report for Contract No. 63-630-8508

Submitted to:

Oregon Department of Geology and Mineral Industries

and the

Gorda Ridge Technical Task Force

Released July 1986

NOTICE

This report is based on results of a research program directed by the joint federal-state Gorda Ridge Technical Task Force, managed by the Oregon Department of Geology and Mineral Industries, and funded by the Minerals Management Service, U.S. Department of the Interior, through Cooperative Agreement. Opinions expressed are those of the authors and do not constitute endorsement by the sponsoring agencies or the Task Force.

The Oregon Department of Geology and Mineral Industries is publishing this paper because the subject matter is consistent with the mission of the Department. To facilitate timely distribution of information, camera-ready copy submitted by the authors has not been edited by the staff of the Oregon Department of Geology and Mineral Industries.

TABLE OF CONTENTS

LIST OF FIGURES

LIST OF TABLES

HYDROTHERMAL SULFIDES, BRECCIAS, AND GREENSTONES FROM THE GORDA DEPRESSION

Roger Hart, Douglas Pyle and James Robbins
College of Oceanography
Oregon State University
Corvallis, Oregon, 97331

ABSTRACT

Three distinct stages of hydrothermal mineralization are represented in samples recovered by dredging along the Blanco Transform Fault in the Gorda Depression. Disseminated pentlandite, pyrrhotite, and pyrite apparently formed at high temperatures in gabbros by precipitation from hydrothermal solutions chemically similar to seawater with stripping of Mg, Ni, and Cr from the seawater and leaching of Cu, Zn, and Pb from the oceanic crust. Secondly, mature hydrothermal solutions laden with dissolved chemicals formed chlorite and epidote rich veins in basalt and breccia with concurrent precipitation and fragmentation of chalcopyrite, sphalerite, and pyrite. Relative to MORB these veins and brecciated zones are enriched in Ag, Cu, Zn, Pb, and Co, and depleted in Sc, Ni, and Cr. The last stage of hydrothermal mineralization was accompanied by precipitation of silica rich phases in veins and breccia zones with precipitation of bornite, chalcopyrite, pyrite, sphalerite and galena. The silica veins are also enriched in Ag, Cu, Zn, Pb and Co, and depleted in Cr, Ni, and Sc. The data suggest the hydrothermal mineralization ocurred in a dynamic regime of changing temperature and water/rock ratio under sufficient pressure to produce incipient brecciation and re-opening of veins and fractures.

INTRODUCTION

In August of 1985 more than twenty kilograms of hydrothermal sulfides, breccias and greenstones were recovered by the USGS vessel R/V Lee in three dredge hauls in the Gorda Depression at the nothern end of the Gorda Ridge. Detailed chemical, mineralogical and petrological studies indicate these samples are typical of stockwork zones associated with massive sulfides in Phanerozoic and Archean ophiolites (uplifted ocean floor tectonically emplaced on continental margins).

Chemical exchange between seawater and oceanic crust was first documented in volcanic rocks dredged from the seabed and traced through volcanic piles up to 7 km thick in Phanerozoic ophiolite sections (Hart 1970, Hart 1973a, b, Thompson 1973, Hart et al., 1974, Spooner and Fyfe 1973, Spooner et al., 1977, Coisch 1977, Humphris and Thompson 1978a, b, Liou and Ernst 1979, Cocker et al., 1982, , Elthon 1981, Elthon et al., 1984, Stakes and O'Neil 1982, Alt et al., 1985, Honnorez et al.,1985). These studies revealed a picture of highly variable chemical metamorphism within the oceanic crust reflecting high geothermal gradients, variable oxidation states and fluctuating water to rock ratios. A composite section is reproduced here for reference in figure 1. Low temperature alteration and formation of open lattice clay, mica and zeolite dominates in the upper 500 m of pillow basalts and is typified by enrichments of the alkalis (Li, Na, K, Rb, Cs), oxidation of iron and leaching of Mg in exchange for Ca and Si (Hart 1973a, Hart et al., 1974, Thompson 1973, Donnelly et al., 1979, Hart and Staudigel 1982). Greenschist facies metamorphism dominates in the lower pillow lavas, sheeted

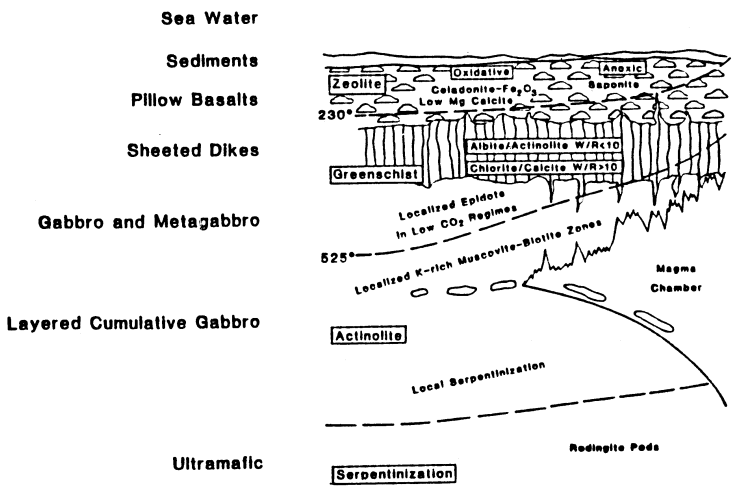

Figure 1: Schematic representation of principal metamorphic regimes associated with an active oceanic spreading ridge. Configuration of the magma chamber is from the work of Gregory and Taylor (1981). Principal isotherms, based on oxygen-isotope estimates of mineral stability fields, are from Spooner et al. (1977); Cocker et al. (1982); Elthon et al. (1984); Alt et al. (1985). The observation of albite-actinolite stability at W/R ratios less than 10 and chlorite-calcite W/R ratios greater than 10 is based on the hydrothermal experiments of Seyfried et al. (1978). The suppression of epidote by the presence of CO_2 is based on observations by Bass et at. (1973). The presence of K-rich micas in the actinolite facies zone is based on observations in the Sarmiento ophiolite by Stern and Elthon (1979). Pods in the gabbro zone represents cumulates.

dikes and occasionally the underlying massive gabbros. Amphibolite or actinolite facies metamorphism occurs mainly in the lower sheeted dikes and massive gabbros at depth in the section, occasionally reaching temperatures in excess of 525°. These high temperature phases are typified by enrichment of Mg thought to be stripped from seawater in exchange for Si and Ca (Hart 1973a, b, Humphris and Thompson 1978a, deWit and Stern 1976). Under special conditions of spillite formation at low water/rock ratios Na and Si are stripped from seawater with Mg.

The stripping of Mg from seawater at high temperatures within the oceanic crust was dramatically confirmed by chemical analyses of hot spring effluents from the Galapagos Rise, East Pacific Rise and Guaymas Basin (Corliss et al., 1979, Edmond et al., 1979a, b, VonDamm et al., 1985a, b). In regards to metallogenesis within the oceanic crust the hot spring chemical studies revealed several other important points. First, free oxygen and sulfate radicals are stripped along with Mg, suggesting seawater becomes more reducing as it evolves into hydrothermal solutions. Secondly, Ni and Cr are removed (Edmond et al. 1979a) yet the sink for these strategic metals has not yet been identified in the oceanic crust. Lastly, Cu, Zn, Fe, Mn, Co, Cd, Pb and Ag are enriched in the effluents that exit at hydrothermal vents.

The first documentation of massive sulfides associated with marine hydrothermal system was made at the Troodos Ophiolite (Spooner and Fyfe 1973). Ocean floor affinity has now been attributed to massive sulfides in the ophiolite complexes of Oman, Saudi Arabia, Turkey, Newfoundland, Corsica, Solomon Islands, Phillipines, the Klamath Mountains of Oregon and northern California and the Appenines of Italy (Spooner and Fyfe 1973, Constantinou 1980, Sangster 1980, Coleman et al., 1978, Ferrario and Garuti 1980, Jankovic 1980, Koski and Derkey 1981). While most of these massive sulfides have been mined since antiquity, they are now only of marginal economic importance. In contrast to the Phanerozoic ophiolites mentioned above, the Archean ophiolites in the greenstone terranes of the Canadian, Southern African, Australian and United States pre-cambrian shields contain many economically fertile deposits. Archean subseafloor hydrothermal systems have been documented at the Noranda, Mattagami, Amulet, Agnico-Eagles and Lower Kam deposits of Canada; the Onverwacht, Peitersburgh and Nondweni localities of South Africa; the Kalgoorlie district of Western Australia and the Atlantic City region of Wyoming (MacGeehan and MacLean 1980, Roberts and Reardon 1978,

Beatty and Taylor 1980, deWit et al., 1982, Hart and deWit 1984, deBeer et al., 1986, deWit et al., 1986, Fripp 1986, Martyn 1986, Harper 1986, Helmstaedt and Padgham 1986, Hunter et al., 1986).

The hydrothermal origin of massive sulfides in ophiolitic assemblages within greenstone belts was dramatically confirmed by the discovery of massive sulfide mounds, hydrothermal vents and actively growing chimneys in the East Pacific Rise and Guaymas Basin (Francheteau et al., 1979, Spiess et al., 1980, Hekinian et al., 1980, Lonsdale et al., 1980). Similar systems were later found on the Galapagos Rift, Juan de Fuca and Explorer Ridges (Malahoff 1981, 1982, Normark et al., 1982, Koski et al., 1982, Koski et al., 1985a, b). The possible economic significance of these ridge crest deposits was encouraged by reports, based on visual observation on Alvin traverses, of 20 million tons of copper bearing ore on the Galapagos Ridge valued at an estimated $2 billion dollars (Malahoff 1982, Bischoff et al., 1983).

Rona (1976) suggested that the discharge from ridge crest geothermal systems is concentrated in the deep fractures at the rift valley margins and that considerable deposition takes place in the fault traces. This suggestion is consistent with observations in Phanerozoic and Archean ophiolites that many massive sulfide deposits occur in chloritized or serpentinized fissure zones cutting the upper sheeted dikes and lower pillow basalts (Franklin et al., 1981). Indeed, fault scarps offer an independent source of thermal energy, the hydration of peridotite by seawater. Hydration of periodite,and most other igneous rocks, is exothermic with heats of reaction in the range -16 to -61 kcal/mole. Fyfe and Lonsdale (1981) calculate the serpentinization of 1 km^3 of peridotite by hydration would evolve about 2 x 10^{17} cal and raise the temperature of the entire body to 200°C.

Evidence of active hydrothermal activity within fault zones has been provided from a number of disciplines. Bonatti et al., (1976) found pyrite concretions in the Romanche Fracture Zone. Vidal et al., (1978) described an offshore hydrothermal field with exit effluent temperatures of 104°C where the San Andreas fault system, intersects the Pacific coast of Baja California at Punta Banda. A ^3He anomaly was detected on the Charlie-Gibbs transform fault by Jenkins and Clarke, (1976). Inactive hydrothermal vents have been described in Fracture Zone A at 37°N on the Mid-Atlantic Ridge (Hoffert et al., 1978; Lalou et al., 1977). Small positive temperature anomalies were measured in the Siqueiros transform fault (Crane 1976). Metalliferous sediments have been found in the Blanco depression of the Blanco Fracture Zone (Selk 1977). Large methane anomalies have been detected in both the Blanco depression and the Cascadia depression to the west of the Gorda depression (Masoth 1985, personal communication). Thus, fault scarps are not only windows into the deeper sections of the oceanic crust where the deeper portions of hydrothermal system can be investigated, they are also possible focal points of hydrothermal activity and massive sulfide deposition.

In order to test this hypothesis, a dredge program was designed and carried out in collaboration with Dr. David Clague of the USGS and funded by the Gorda Ridge Task Force in the summer of 1985. All three dredge attempts on the northern face of the Gorda Depression collected hydrothermal material. In this report we first describe the analytical and sampling procedures, then discuss the hydrothermal material from a megascopic and microscopic perspective and finally discuss the results of extensive chemical analyses and the general problem of hydrothermal metallogenesis in fault scarps.

ANALYTICAL METHODS

Dredge samples collected from the Gorda Depression were powdered, and analyzed for major and trace elements by Instrumental Neutron Activation

Analysis (INAA) and Atomic Absorption Spectroscopy using both flame (FAAS) and heated graphite atomization (HGA) techniques. Major mineral constituents and alteration products were determined petrographically and corroborated with x-ray diffraction (XRD) results.

After removing oxidation, the interiors of the rock samples were crushed in a jaw crusher and sieved. Next, the rock chips were washed with distilled-deionized water in an ultra-sonic bath, rinsed several times, and placed in an oven to dry. This procedure removes any dust not separated from the sample by the seiving and insures the rock chips are clean and uncontaminated. The whole rock chips were then split and powdered in a tungsten-carbide ball mill for approximately 15 minutes.

The majority of trace elements were determined by INAA. 500 mg aliquots of the whole rock powders were placed in acid washed 2/5 dram polyvial and sealed with a hot iron. The 2/5 dram polyvials were then incapsulated and hot-iron sealed in 2 dram polyvials and irradiated at the Oregon State University Radiation Center in a TRIGA reactor. The samples were subjected to a 7 hour bombardment period in the "Lazy Susan" rotating rack surrounding the reactor core. Rotation of the samples during irradiation ensures samples and standards are exposed to the same thermal neutron flux ($\sim 3 \times 10^{12} n/cm^2 sec$) during irradiation. After the samples are allowed to decay for 2-3 days, the counting scheme outlined below was followed:

Count Period	Decay from EOB*	TOC	half-life	Elements
1	2-3 days	5 mins	<20 hrs	K, NA
2	4-6 days	2-3 hrs	1-10 days	La, Sm, Lu, U, Au, Yb, As, Sb
3	1-2 weeks	3-4 hrs	10-20 days	Nd, Ba, Rb
4	3-4 weeks	4-8 hrs	>20 days	Th, Cr, Ce, Hf, Fe, Tb, Sc, Ta, Cs, Co, Eu, Sr, Se, Ag, Ni

* End of bombardment
† Time of Count

The gamma-ray energy spectra for each sample was collected by a Ge(Li) detector connected to a Nuclear Data (ND66) multichannel analyzer calibrated to .415 Kev/channel with an energy resolution of 2.5 Kev/channel at 1332 Kev. Peak searches and peak settings were done visually and total, net, and background counts for each peak was transfered and stored on files for later data reduction on a Dec PDP11/23 Computer system. Visual peak setting has the advantage over computer automated peak assignments in that smaller than usual peaks and interference correction judgments are more easily determined.

All major elements and some trace elements were determined by Atomic Absorption. 200-300 mg of sample powder were dissolved in 8 ml of 1:1 HF-HNO_3 acid mixture over night in a 60°C oven. Flourides which form during the dissolution of the samples were redissolved into solution by adding 50 ml of a 4% boric acid solution and returned to the oven for additional 1-2 hr. To this solution 2 ml of CsCl (50,000 ppm) was added as an ionization suppressant and 40 ml of distilled-deionized water was added to complete the 100 ml dilution of the sample. All major elements were determined by conventional flame AA on a Perkin-Elmer 5000, as were Sr, Ba, Rb, Li, Cu, Ni, and Zn. Concentrations of Pb and Ag were not detectable by FAAS so heated graphite atomization was employed. The Perkin-Elmer 5000 is equipped with a

HGA furnace with Zeeman background correction that allows for picogram detection capabilities in very complex matrixes. Water and carbon-dioxide values were determined using a Perkin-Elmer 240C elemental carbon-hydrogen-nitrogen analyzer.

Major minerals and some alteration products were determined petrographically but identification of some minor mineral phases could only be done by XRD. Whole rock powders were smear mounted on aluminum discs and analyzed on a Scintag PADV x-ray diffractometer equipped with a copper target x-ray tube, operated at 40 KV-30Ma, connected to a solid state germanium detector. Diffraction patterns were time averaged scans between 30-80° at a scan rate of 20°/min. Each pattern is the result of 25-30 complete scans. Time average scanning enhances the signal to noise ratio of the defraction pattern and provides a clearer separation of real peaks from background scatter. The XRD software automatically performs a 3 point smoothing function on the raw x-ray data and the patterns used in our evaluation had an additional 2 point smoothing.

Further chemical characterization of the primary and secondary minerals in the Gorda Ridge samples was done by Scanning Electron Microscopy and detailed Electron Microbeam analyses. SEM work was carried out at both OSU and the Bureau of Mines Research Facility in Albany, Oregon. Microprobe studies were performed under the direction of Michael Schaffer at the University of Oregon Microbeam Laboratory. They are equipped with an ARL EMX-SM electron probe microanalyzer (EPMA) with Tracor Northern automation. Run conditions for silicates were set to 15 Kev operating voltage, 15 namp sample current with a 5 μm defocussed spot size and Bence-Albee corrections applied. Sulfide run conditions were set to 15 Kev operating voltage, 20 namp sample current with a 1μm focussed spot size and ZAF corrections applied.

Figure 2: SeaBeam countour map of the Gorda Depression region of the Blanco Fracture Zone showing dredge traces. Map provided by Dr. Robert Embley.

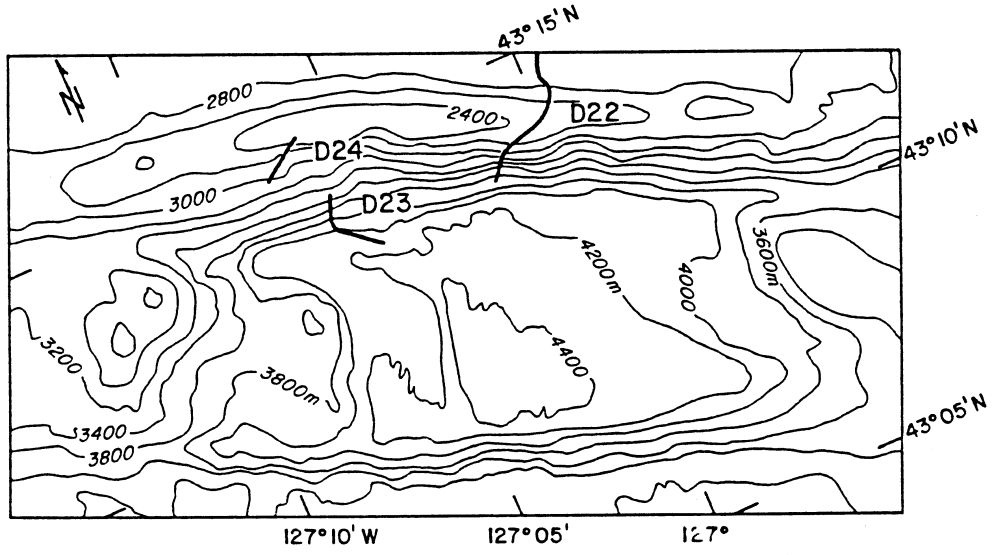

SAMPLE DESCRIPTIONS

The samples were dredged from the north wall of the Gorda Depression in August of 1985 by the USGS ship R/V Lee. The dredge targets were located on a 100% coverage seabeam map based on data collected on the NOAA ship R/V Surveyor in the summer of 1983 (Embley, personal communication). The dredge locations are shown in Fig. 2 and pertinent data presented in table 1. For ease of description, the samples have been classified into four catagories: altered basalts, greenschist gabbros, greenschist breccias, and siliceous samples. A summary of the petrology and mineralogy is given in table 2.

Table 1. Dredge Locations in the Gorda Depression

Dredge Number	Location		Depth		OSU Sample Nos.
	Start	End	Start	End	
L5-85-NC-22D	43°12.93'N 126°01.78'W	43°14.48'N 126°59.53'W	3800m	2577Om	RHGR-1 RHGR-2 RHGR-4 RHGR-8 RHGR-15 RHGR-16 RHGR-18 RHGR-21 RHGR-23 RHGR-24 RHGR-25
L5-85-NC-23D	43°12.54' 127°06.18'	43°13.94' 127°05.97	4100m	3500m	RHGR-26
L5-85-NC-242	43°13.85 127°08.48'	43°15.078' 127°06.78'	2900m	2300m	RHGR-3 RHGR-5 RHGR-6 RHGR-11 RHGR-13 RHGR-22

Altered Basalts

Twelve basalts were selected for analysis. All the samples are altered but some observations concerning the original igneous textures can be made. The basalts range from those typical of the glassy margins of pillow basalts to more phaneritic varieties typical of pillow basalt interiors, to coarser grained, doleritic types perhaps from intrusive sills or dikes. The glassy basalts are holohyaline to hypohyaline with frequent tachytic mottling. The phaneritic basalts are porphyritic with plagioclase in tabular laths or acicular needles, variolitic with aggregates of plagioclase, or subophitic with intergrowths of plagioclase and augite. Plagioclase, where fresh, is typically labradorite and often the augite displays pleochroism typical of high Ti varieties. Euhedral olivines pseudomorphed by antigorite are present in the phaneritic varieties. The most common accessory mineral is ilmenite often altered to leucoxene. Secondary carbonates, ankerite and calcite, were observed. The main sulfides are chalcopyrite and pyrite and occur both disseminated in the groundmass and in chlorite veins. Assuming the sulfur is mainly in sulfides, the total sulfide concentration in basalts reaches greater than 2%.

The most common metamorphic phases are albite and various chlorite-type minerals. The albite most commonly replaces plagioclase but has also been

Table 2. Sample Descriptions

Sample No.	Hand Specimen	Thin Section	X-ray Diffraction	Microprobe
		ALTERED BASALTS		
RHGR-1	Greenish-gray subophitic pillow basalt fragment with 1-2% dissiminated sulfides and spherical cavity fillings of dark green chlorite mineral.	Albitized plagioclase and uralitized augite, ilmenite, pyrite and chalcopyrite, possible euhedral olivines replaced by chlorite.	Albite, augite, pyrite, ilmenite, leucoxene, clinochlore, chalcopyrite.	albite, clinochlore actinolite, pyrite.
RHGR-3	Dark-green metamorphosed aphanitic pillow basalt interior irregular patchy texture with abundant sulphide both disseminated and in veins.	Plagioclase altered to smectite and albite; uralitized augite, groundmass filled with patches of chlorite.	albite, augite, pyrite clinoclore.	albite, clinochlore actinolite, pyrite.
RHGR-4	Porphyritic pillow basalt with tachylitic glass, veinlets with sulfides.	"Swallowtail" plagioclase (labradorite), clinopyroxene with minor uralitization, tachylitic glass matrix, vesicles filled with penninite; veins lined with laumontite and filled with penninite, prehnite, and calcite; abundant chalcopyrite and pyrite.	Ca-plagioclase, augite clinoclore, laumontite, chalcopyrite.	laumontite, clinochlore, chalcopyrite, prehnite.
RHGR-5 (host rock)	Subophitic pillow basalt wedge with veins of brecciated material with abundant sulfides (see below for description of vein material).	albitized plagioclase, augite, euhedral olivine replaced by chlorite.	albite, augite, pyrite, chalcopyrite.	albite, clinochlore chalcopyrite.
RHGR-8	Green subophitic pillow basalt fragment with abundant disseminated sulfides.	Tabular plagioclase, clinopyroxene with incipient uralitization. Clots of chlorite and epidote in groundmass. Veins filled with quartz, minor epidote and dissimenated pyrrhotite.	albite, augite, clinoclore, epidote, pyrrhotite.	clinochlore, epidote pyrrhotite.
RHGR-13	Greenish gray porphyritic pillow basalt fragment with abundant veins of calcite.	large grains of plagioclase altered to albite, uratilized augite, groundmass altered to chlorite, veins of calcite with chalcopyrite.	albite, augite, clinochlore, actinolite, calcite.	albite, actinolite.
RHGR-15	Greenish gray aphanitic pillow basalt interior with trachylytic groundmass.	plagioclase altered to smectite and albite; augite uralitized to actinolite; groundmass altered to chlorite.	albite, augite, clinoclore, pyrite.	albite, pyrite.
RHGR-18	Green porphyritic pillow basalt interior with large phenocrysts of plagioclose.	plagioclase (~AN_{70}), altered to smectite and albite; augite altered to actinolite, tachylytic glass matrix.	anorthite, augite clinochlore, pyrite.	pyrite.
RHGR-21	Olive green basalt fragment with unusual "tectonite" texture.	albitized plagioclase laths cutting "colloform" bands of chlorite and laumontite with minor sphene, actinolite and saponite.	albite, sphene laumontite, actinolite clinochlore.	albite, sphene, saponite, actinolite.
RHGR-23	Variolitic olive green pillow basalt interior fragment.	albite with cores of labradorite, groundmass altered to saponite zones of spotted alteration of chlorite and fibrous actinolite; disseminated pyrite veins filled with laumontite.	albite, clinochlore, laumontite.	albite, clinochlore.
RHGR-24	Olive green variolitic glassy pillow basalt wedge. Tachylytic mottling.	Variolitic bunches of plagioclase altered to albite, with minor epidote. groundmass cut by pumpellyite veins postdate groundmass alteration and are filled with laumontite, prehnite and chlorite; veins contain chalcopyrite.	albite, clinochlore, epidote, prehnite, laumontite, chalcopyrite.	albite, clinochlore, chalcopyrite, laumontite.

RHGR-26	Coarse grained olivine basalt pillow wedge with hologhaline rind, hyalopilitic and variolitic inner zones with intergranular core.	Fresh labradorite and Ti-augite, olivine replaced by brownish green serpentine.	Ca-plagioclase, augite.	labradorite, augite.
		GREENSCHIST GABBROS		
RHGR-2	Greenstone gabbro fragment (12x10x8cm) with lathes of plagioclase up to 4.5mm long and augite up to 2.5mm long abundant voids filled with chlorite and actinolite with associated sulfides.	Labrodorite with incipient alteration to smectite, augite with marginal alteration to fibrous actinolite. ilmenite altered to leucoxene. Voids filled with penninite and fibrous radiating actinolite. Disseminated pyrrhotite and pentlandite associated with secondary void fillings, irregular blobs of goethite after ankerite, veins of secondary albite and laumontite.	Ca-plagioclase clinochlore, augite pyrrhotite, pentlandite.	Ca-plagioclase augite, clinochlore, pyrrhotite, pentlandite analcite veins.
RHGR-16	Greenstone subophitic gabbro with coarse plagioclase (up to 2mm) and augite (up to 2.5 mm).	plagioclase replaced by smectite. subophitic plates of augite replaced by actinolite and chlorite. equant patches of antigorite; veins filled with laumontite and prehnite and disseminated pyrite.	clinochlore, actinolite pyrite, prehnite, laumontite.	actinolite, albite pyrite, prehnite, laumontite.
		GREENSCHIST BRECCIAS		
RHGR-5 veins	Dark green vein filling in pillow basalt fragment. Fragments of basalt, carbonates and matrix material obvious in vein, abundant pyrite, chalcopyrite, and sphalerite.	Fragments of basalts same as given above for RHGR-5 (host rock).Vein matrix epidote, clinochlore, saponite with minor carbonate and quartz. Multiple stages of in-situ brecciation evident down to individual crystals. Brecciation of pyrite, chalcopyrite and sphalerite minerals during formation suggests dynamic conditions.	clinochlore, epidote, albite, dolomite, calcite, ankerite, pyrrhotite, chalcopyrite pyrite, sphalerite.	epidote, pycnochlorite calcite, quartz, pyrite, chalcopyrite sphalerite.
RHGR-22	Greenstone breccia fragment (30x23x17cm) with rounded clasts of greenschist altered basalt cemented with chlorite, zeolites, and clay minerals.	Subophitic basalt fragments as described above with plagioclase altered to albite, and augite partially replaced by actinolite and penninite. Fragments cemented with penninite and saponite cut by veins of laumonite, disseminated pyrite, and small veinlets of antigorite.	clinochlore, albite, augite.	penninite, albite, pyrite, antigorite.
RHGR-25	Brown-green breccia with rounded fragments of basalt cemented by chlorite, clay and serpentine minerals.	Variolitic basalt fragments.	augite, albite, clinochlore.	albite, pyrrhotite, antigorite.
		Siliceous Samples		
RHGR-6	Fragments (up to 2cm) of subhedral quartz with inclusions of albite, and sulfides.	Euhedral and subhedral quartz up to 1mm. Sphene and albite with abundant sulfides mostly chalcopyrite with minor bornite and sphalerite.	quartz, albite, chalcopyrite, bornite, galena.	bornite, chalcocite, chalcopyrite, sphalerite, galena, hematite.
RHGR-11	Fragments (up to 5cm) of a siliceous breccia with fragments of greenstone basalts cemented by amorphous silica (chert).	Cryptocrystalline quartz veins repeatedly opened and refilled, cementing sub-round to angular clasts of altered basalt and occasionally carbonate; In-situ fragmentation and cementation of basalt clasts readily apparent. Sulfides, pyrite and chalcopyrite, mainly associated with basalt fragments.	quartz, albite, chalcopyrite, pyrite clinochlore.	albite, clinochlore, quartz, calcite.

observed in veins. The chlorite minerals most commonly replace the groundmass but also occur as intergrowths in augite and plagioclase, vesicle and vein fillings, and as subround blebs reminiscent of spotted alteration in massive sulfide deposits. Under polarizing light the chlorite minerals vary from typical grayish blue to striking "berlin blue" typical of iron rich varieties such as brunsuigite and ripidolite. The x-ray diffration studies identified both clinochlore and Fe-clinochlore (pycnochlorite). Microprobe analysis indicates the FeO content of the chlorites in the basalt range from a low of 13% to a high of 24% with the highest FeO contents associated with chlorites found as late stage vein fillings.

In the basalts, actinolite occurs as acicular intergrowths within chlorite in vesicle fillings and as feathered edges on augite. Laumontite is a common vesicle and vein filling, often showing late stage fracturing and in filling by chlorite. Epidote is a common vein filling in the basalts. Saponite occurs as vein linings, vein fillings, and as an alteration product of glass and plagioclase.

Traditional textural nomenclature is inadequate to describe an unusual rock type represented in our collection by RHGR-21. Chlorite, sphene, actinolite, and laumontite form alternating .5 mm thick bands enclosing subangular areas rather than rounded ones as in traditional obicular and colloform banding. Furthermore, as shown in Fig. 3, the bands are parallel to intersecting microfractures reminescent of tectonites. Yet, traditionally tectonites are ultramafic in composition whereas this sample has only 10.1% MgO. Microprobe analysis of the bands are given in table 3. A similar texture with smectite bands intergrown parallel to microfractures in glass was described in glassy basalt from DSDP site 417A by Juteau et al (1979). For want of a better term, we will refer to this sample as a mafic tectonite as it is composed of alteration minerals that apparently formed in successive bands adjacent to a microfracture network. The mafic tectonites have little original igneous mineral left and, as indicated by high H_2O (5.76%), are among the most altered samples from the Gorda Depression.

Table 3. Microprobe results for "Mafic Tectonite" RHGR 21 (see Fig. 3 for spot locations)

	Spot 1 clinochlore adjacent to microfracture	Spot 2 clinochlore adjacent to microfracture	Spot 3 albite bleb cutting banding	Spot 4 sphene in translucent band	Spot 5 sphene in translucent band
SiO_2	29.11	29.33	66.90	29.31	30.21
TiO_2	.92	.04	.04	36.86	36.55
Al_2O_3	15.24	16.50	19.42	4.56	5.61
FeO	18.68	19.31	.26	3.48	4.31
MnO	.43	.42	.05	.05	.08
MgO	19.01	20.86	.06	1.09	1.12
CaO	.09	.11	.31	22.39	20.20
Na_2O	.27	.25	11.44	.14	.07
K_2O	.29	.29	.06	.15	.15
Extra Oxygen*	16.01	12.89	1.45	1.94	1.70

	Spot 6 Ca-clinochlore opaque lining on band	Spot 7 clinochlore central core	Spot 8 albite bleb in central core	Spot 9 laumontite in vein	Spot 10 laumontite in vein
SiO_2	29.31	29.58	63.97	53.25	56.93
TiO_2	.14	.04	.04	.03	.02
Al_2O_3	13.59	16.19	17.81	22.84	23.14
FeO	14.28	19.11	.20	-	-
MnO	.48	.41	.05	-	-
MgO	19.93	20.91	.06	-	-
CaO	6.34	.13	1.18	11.22	11.96
Na_2O	.27	.25	11.44	.14	.07
K_2O	.19	.23	.06	.06	.04
Extra Oxygen	15.50	13.11	5.16	12.47	7.84

* Extra oxygen could be oxides, hydroxide, or H_2O.

Figure 3: Schematic representation of texture of mafic tectonite (RHGR-21) with locations of microprobe analysis given in table 3. The alternating bands are chlorite, and sphene (clear zone), with inclusion of actinolite and albite and veins of laumontite. Scale bar represents 1mm.

Basalt Chemistry

The original chemistry of the basalts has been altered by hydrothermal metamorphism; however, the REE, TiO_2, Al_2O_3 and Hf, concentrations are typical of mid-ocean ridge basalts (MORB). The major element concentrations are given in table 4, the metallic trace elements in table 5, the lithophile trace elements in table 6, and the rare earth elements in table 7.

Among the major elements, those that show the most consistent variability as a result of hydrothermal metamorphism are SiO_2, CaO, and MgO. Fig. 5 shows a negative correlation between SiO_2 and CaO and H_2O and a positive correlation between MgO and H_2O. These trends are typical of chlorite dominated hydrothermal alteration in the greenschist facies above 200°C at water/rock ratios in the range 10-100 (Hart 1973 a, b; Seyfried et al 1978; deWit et al.1986). Sample RHGR-24 has elevated SiO_2 and Na_2O contents suggesting it is a spillite formed in the greenschist facies at water/rock ratios less than 10 (Hart 1977a, Seyfried et al 1978). Although K_2O shows no systematic correlation with H_2O, RHGR-8, RHGR-13, RHGR-21, and RHGR-22 show clear K_2O enrichments indicating formation of open lattice clays and micas at temperatures below 200°C. These same samples are enriched in Rb. Among the other trace elements, only Sr show a significant variation with alteration and shows definite depletion in the ultramafic tectonite sample (RHGR-21) thought to have formed in the greenschist facies at moderately high water/rock ratios.

Gabbros

The gabbros consist mainly of laths of plagioclase (An63 where fresh) up to 4.5 mm long in plates of subophitic augite crystals up to 2.5 mm long. Minor ilmenite and pyrrhotite, with scarce pentlandite, are disseminated throughout the gabbros. Assuming the sulfur is in sulfides, the total sulfide content ranges between 1.5 and 2.0%. Microprobe analysis of sulfides are given in table 9. The plagioclase is dominantly replaced by albite and saponite. The augite is pervasively altered to actinolite and chlorite. Rare patches of antigorite replace olivine. Voids are filled with chlorite and radiating needles of actinolite, forming patches suggestive of spotted alteration. Veins are lined with chlorite and prehnite and filled with laumontite. The texture of the greenschist gabbro is shown in Fig. 6. Chemically, the gabbros are similar to basalts with a slight REE depletion. The effects of alteration on the chemistry are much less pronounced with only minor enrichment of MgO and depletion of SiO_2 and CaO compared to average MORB.

Table 4. Major Element Concentrations in Gorda Depression Samples (Weight %)†

Sample No.	SiO_2	TiO_2	Al_2O_3	Total Fe as Fe_2O_3	MnO	MgO	CaO	Na_2O	K_2O	CO_2	H_2O	P_2O_5	*S	Total
ALTERED BASALTS														
RHGR-1	47.60	1.92	14.10	11.01	.29	8.22	8.12	1.96	.13	.02	4.62	.14	.86	98.99
RHGR-3	41.10	2.04	15.42	16.87	.38	11.76	2.24	1.54	.21	.08	6.73	--	--	98.41
RHGR-4	50.60	1.87	14.10	11.24	.42	7.79	9.44	1.86	.07	.04	2.32	.13	--	99.95
RHGR-5H	46.50	1.56	14.74	10.47	.33	8.73	9.28	1.83	.14	.05	3.60	.13	.09	97.40
RHGR-8	48.20	1.74	14.18	10.44	.24	8.60	8.01	1.67	.39	.04	3.95	.14	.40	98.00
RHGR-13	48.70	1.75	14.12	10.45	.26	9.36	7.42	1.74	.42	.05	2.82	.12	--	97.15
RHGR-15	48.30	1.82	14.16	10.44	.30	8.03	7.45	2.17	.15	.05	4.22	.13	.24	97.46
RHGR-18	47.90	1.82	15.78	9.35	.25	7.95	9.76	1.48	.14	.04	3.47	.11	.96	99.73
RHGR-21	44.90	1.80	16.33	14.01	.37	10.71	3.88	1.78	.40	.04	5.76	.13	--	100.11
RHGR-23	50.00	1.38	14.69	10.88	.25	8.65	9.69	1.64	.29	.05	2.50	.10	--	100.12
RHGR-24	53.50	1.92	13.34	10.84	.52	8.65	9.69	2.56	.29	.05	3.14	.14	--	97.93
RHGR-26	50.20	1.47	16.18	8.78	.28	7.04	11.55	1.64	.12	1.34	.98	.20	.15	99.93
GREENSCHIST GABBROS														
RHGR-2	47.60	1.82	15.20	9.84	.28	7.47	9.49	1.85	.21	.04	3.55	.14	.93	98.42
RHGR-16	51.60	1.61	12.87	9.57	.20	8.23	7.21	2.28	.21	.09	3.92	.12	--	97.91
GREENSCHIST BRECCIAS														
RHGR-5V	39.00	1.01	17.50	13.97	.36	5.69	12.60	.96	.17	.46	5.45	--	--	97.17
RHGR-22	50.40	1.28	14.61	9.70	.41	9.44	7.08	2.34	.33	.49	3.31	.10	.13	99.62
RHGR-25	49.90	1.42	14.97	10.37	.30	9.21	6.90	2.34	.10	.22	3.53	.11	.01	99.35
SILICEOUS SAMPLES														
RHGR-6	83.00	.41	3.04	6.11	.20	2.67	.45	.07	.01	.07	1.65	--	--	97.61
RHGR-11	74.60	.87	7.28	5.35	.08	3.19	1.23	1.24	.05	.22	3.25	--	--	97.36

† Error as coefficient of variation (S.D./mean x 100), 1-3%
* Semiquantitative XRF determined by extrapolation of calibration curves for abundance below .1%.

Table 5. Metallic Trace Elements (ppm)

Sample No.	Cr	Ag (ppb)	Cu	Ni	Co	Zn	Sc	Au (ppb)	Pb	As	Sb
ALTERED BASALTS											
RHGR-1	207	50	80.9	64	34	105	41.1	--	0.3	--	--
RHGR-3	410	30	183	53	43	197	--	--	1.0	--	--
RHGR-4	154	30	76.4	63	45	124	42.3	1.4	0.4	--	0.07
RHGR-5 H	377	10	61.4	92	39	174	42.8	--	0.2	1.8	--
RHGR-8	248	60	59.4	67	41	89	45.4	2.8	0.5	--	0.04
RHGR-13	251	--	15.1	68	41	68	44.0	--	0.3	--	--
RHGR-15	248	30	54.9	71	36	152	41.9	1.4	1.1	1.6	0.07
RHGR-18	252	30	11.7	65	41	70	42.7	--	0.2	--	0.10
RHGR-21	148	--	4.0	56	39	212	39.3	1.0	0.2	--	0.03
RHGR-23	269	--	41.7	71	40	76	41.8	--	0.2	--	0.05
RHGR-24	163	--	24.3	83	37	221	43.2	--	4.4	0.7	0.20
RHGR-25	310	--	56.8	79	34	143	39.6	1.4	0.7	--	--
RHGR-26	296	--	60.2	118	37	63	36.7	1.3	0.3	--	0.10
GREENSCHIST GABBROS											
RHGR-2	243	10	91.8	61	35	91	41.6	--	0.1	--	0.06
RHGR-16	383	--	2.7	48	40	27	42.9	--	2	--	.04
GREENSCHIST BRECCIAS											
RHGR-5 V	251	40	550	53	44	678	28.9	--	0.5	--	--
RHGR-22	345	150	117	90	39	73	39.6	2.1	0.2	--	0.06
RHGR-25	310	--	56.8	79	34	143	39.6	1.4	0.7	--	--
SILICEOUS SAMPLES											
RHGR-6	93	810	3610	--	25	621	--	--	0.5	--	--
RHGR-11	119	20	31.4	63	17	68	18.4	--	0.6	1.9	0.19
Error	(5-7%)*	(15-30%)†	(5-10%)†	(2-5%)†	(2-4%)*	(1-3%)†	(1-2%)*	(50-70%)*	(10-20%)†	(50-70%)*	(40-60%)*

† C.V.
* S.D. (3σ) INAA Counting Statistics

Table 6. Lithophile Trace Elements (ppm)

Sample No.	Rb	Sr	Ba	Li	Hf	Th	U
ALTERED BASALTS							
RHGR-1	1	134	30	2.4	2.70	--	0.2
RHGR-3	2	46	30	9.6	--	--	--
RHGR-4	2	109	--	3.1	2.87	--	0.6
RHGR-5 H	2	121	--	4.6	1.93	--	--
RHGR-8	3	121	40	5.7	2.35	--	--
RHGR-13	3	108	50	9.2	2.46	--	--
RHGR-15	2	96	--	7.1	2.49	--	0.2
RHGR-18	1	115	30	1.6	2.40	--	0.1
RHGR-21	2	25	--	7.3	2.61	0.13	0.2
RHGR-23	2	86	--	9.2	1.82	--	0.2
RHGR-24	1	141	--	7.6	2.83	--	0.3
RHGR-26	1	207	--	2.6	2.55	--	--
GREENSCHIST GABBROS							
RHGR-2	2	151	30	2.4	2.30	0.6	0.2
RHGR-16	2	122	--	2.4	2.10	--	0.3
GREENSCHIST BRECCIAS							
RHGR-5 V	--	82	--	3.9	1.36	0.06	0.1
RHGR-22	1	88	--	4.9	2.14	--	--
RHGR-25	1	92	--	10.3	1.79	0.05	0.1
SILICEOUS SAMPLES							
RHGR-6	1	6	30	24.5	--	--	--
RHGR-11	1	33	--	41.5	1.54	0.03	--
Error	(5-10%)†	(2-3%)†	(3-4%)†	(1-3%)†	(5-10%)*	(30-50%)*	(40-60%)*

† C.V. AA
* S.D. (3σ) INAA

Table 7. Rare Earth Elements (ppm)

Sample No.	La	Ce	Nd	Sm	Eu	Tb	Yb	Lu
ALTERED BASALTS								
RHGR-1	1.41	8.9	10.2	3.66	1.04	0.82	3.41	0.53
RHGR-4	3.79	9.2	12.1	4.13	1.33	0.83	3.45	0.61
RHGR-5 H	2.42	7.4	7.2	3.08	1.01	0.56	2.82	0.46
RHGR-8	2.82	8.4	8.7	3.60	1.08	0.76	3.04	0.49
RHGR-13	2.80	7.8	8.5	3.35	1.05	0.68	3.34	0.50
RHGR-15	3.43	10.9	9.9	3.61	1.22	0.80	3.37	0.50
RHGR-18	2.62	9.5	6.6	3.50	1.13	0.75	3.35	0.49
RHGR-21	3.80	11.9	11.1	3.60	1.32	0.70	3.49	0.47
RHGR-23	2.16	7.4	7.0	3.04	1.08	0.54	2.51	0.48
RHGR-24	5.50	17.4	10.1	4.70	1.75	0.79	4.19	0.63
RHGR-26	4.93	14.6	10.6	3.63	1.41	0.63	3.19	0.42
GREENSCHIST GABBROS								
RHGR-2	2.94	9.3	8.9	3.45	0.99	0.62	3.37	0.52
RHGR-16	2.70	8.4	9.8	3.15	0.86	0.64	2.85	0.48
GREENSCHIST BRECCIAS								
RHGR-5 V	1.89	6.3	6.8	2.14	1.42	0.44	1.73	0.31
RHGR-22	2.09	6.9	6.9	2.85	1.01	0.58	2.60	0.41
RHGR-25	2.59	7.7	8.0	2.96	1.13	0.59	2.98	0.45
SILICEOUS SAMPLES								
RHGR-11	1.55	6.1	6.5	1.89	0.75	0.50	1.73	0.27
Error	(3-8%)	(4-8%)	(10-15%)	(1-2%)	(5-7%)	(5-8%)	(5-8%)	(5-7%)

All by INAA, S.D. (3σ) counting statistics

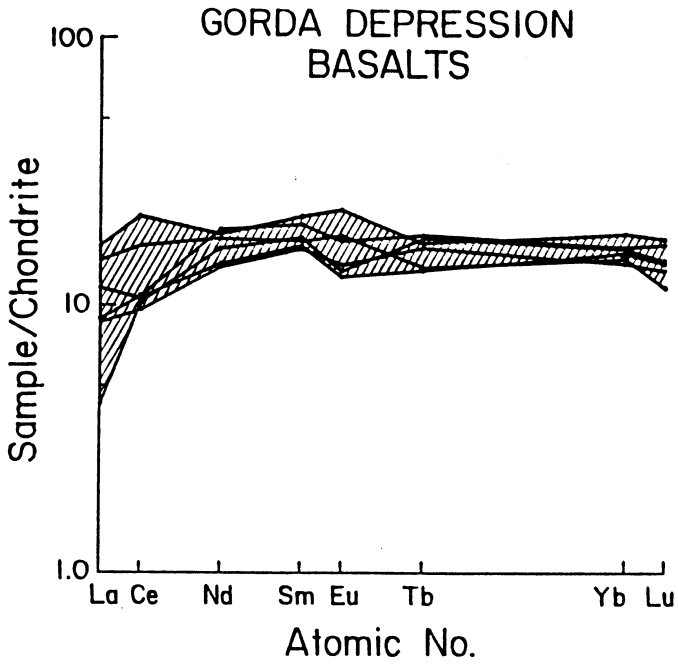

Figure 4: Rare Earth Patterns for Gorda Depression Basalts showing typical MORB patterns.

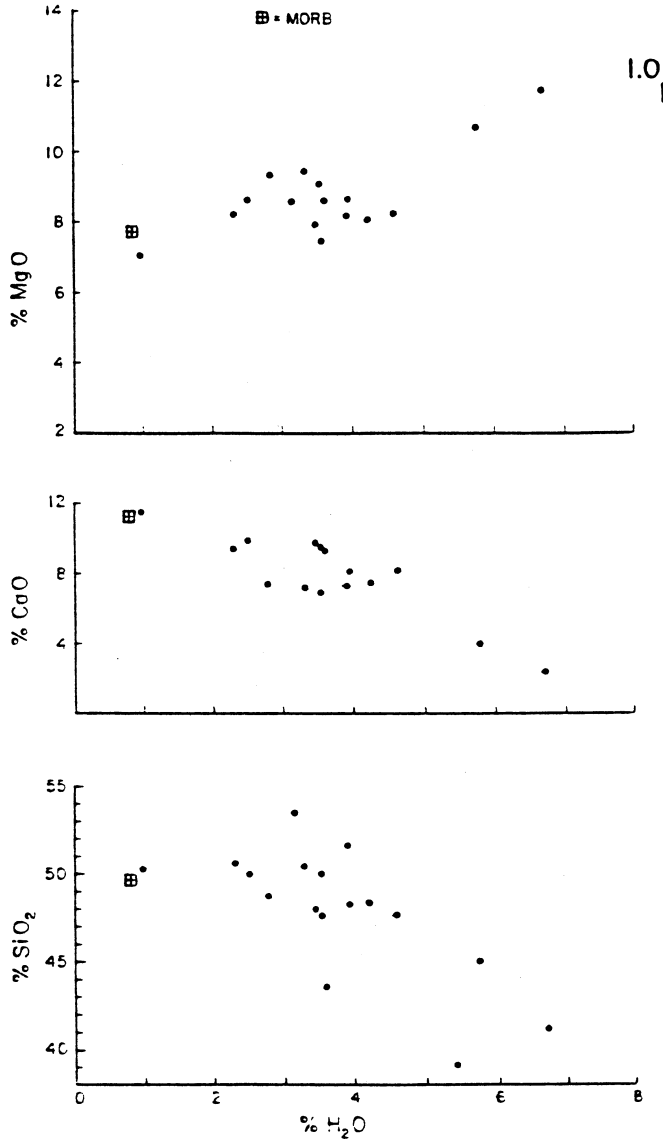

Figure 5: Hydration plots for Gorda Depression basalts are shown with MgO, CaO, and SiO_2 plotted vs. H_2O. The depletions of SiO_2 and CaO indicated in the most hydrated samples are in excess of that predicted by simple dilutions by H_2O.

Figure 6: Reverse image depiction of gabbroic texture in sample RHGR-16. plagioclase in a matrix of subophitic pyroxene now almost completely altered to actinolite. In the middle left of the figure a white vein of actinolite is cutting both albite and pyroxene. Microprobe analysis of this vein, actinolite, albite, augite, and laboradorite are given in table 8 and sulfide minerals in table 9. The scale bar represents 5 mm.

Table 8. Microprobe Analysis of Silicate Minerals in Gabbros

	Augite	Plagioclase	Albite replacing labradorite	Actinolite replacing Augite	Actinolite replacing Augite
SiO_2	49.20	52.94	56.48	48.62	49.16
TiO_2	1.03	.06	.04	.30	.58
Al_2O_3	4.46	28.72	25.19	5.26	4.59
FeO	6.32	.85	.06	13.19	13.72
MnO	.20	.06	.05	.22	.23
MgO	16.46	12.28	.05	15.71	15.49
CaO	20.57	4.21	6.85	10.65	11.54
Na_2O	.30	.13	8.25	1.15	1.10
K_2O	.06	.08	.31	.09	.09
Extra Oxygen	1.40	.07	2.71	4.81	3.49

	Actinolite Vein in augite	Actinolite needles in chlorite spot	Chlorite spot	Penninite spot	Analcite vein
SiO_2	44.47	48.02	27.89	33.18	54.89
TiO_2	.15	.15	.04	.04	.04
Al_2l_3	9.26	8.00	16.94	15.02	23.02
FeO	11.67	24.48	24.84	19.67	.06
MnO	.25	.41	.68	.79	.05
MgO	12.24	9.54	18.32	19.53	.06
CaO	9.56	7.36	.08	.17	.08
Na_2O	1.54	.56	.08	.80	11.66
K_2O	.13	.09	.11	.36	.06
Extra Oxygen	10.73	4.38	10.98	10.54	10.08

Table 9. Microprobe Analysis of Disseminated Sulfides in Greenschist Gabbro (RHGR-2)
XRF sulfur contents suggest total disseminated sulphide is betwen 1.5 and 2.0%

	Pyrrhotite	Pyrrhotite	Pyrrhotite	Pentlandite	Pentlandite
S	57.85	59.36	58.15	37.38	35.16
Cu	.32	.28	.46	.62	.61
Fe	41.30	40.36	41.68	50.23	51.13
Zn	.46	.41	.37	.12	.14
Sb	.07	.08	.06	.05	.04
As	.05	.06	.07	.06	.07
Mn	.11	.09	.10	.09	.08
Ni	.63	1.23	.56	9.46	11.26
Cr	.43	.32	.26	.63	.72

Breccias

Four distinct types of breccias were recovered in the dredges. The siliceous breccia is discussed in the next section.

A hydrothermal breccia depicted in Fig. 7 exhibits matching vein walls and contains fragments of altered basalts that have been displaced only short distances from original positions in the host rock. The matrix is clinochlore and epidote with minor carbonate, sphene, and saponite. Microprobe analysis of the matrix silicates are given in table 10. Pyrite, chalcopyrite, and sphalerite are common and typically display fragmented growth patterns suggesting they crystallized in a dynamic environment. Microprobe analysis of the sulfides are given in table 11. The basalt fragments are often subrounded suggesting attrition by fluids under high pressure as described by Delaney et al. (1986) for hydrothermal breccias from the Mid-Atlantic Ridge. Because this breccia is enclosed by a host rock it offers an opportunity to study the depletion-enrichment characteristics of hydrothermal mineralization. As shown in Fig. 8, SiO_2, TiO_2, MgO, and Na_2O are depleted in the vein compared to the host basalt. To a large degree these are apparent depletions caused by a dilution effect by enrichments in Al_2O_3, FeO, and CaO. The abundance of these elements reaches values significantly higher than in any unaltered MORB, and provides evidence of Al_2O_3 FeO, and CaO precipitation from hydrothermal solutions.

The REE concentrations of the vein and host rock are virtually identical (Fig. 9) with the exception of Eu which shows enrichment in the vein, perhaps because of substitution of Eu for Ca in epidote or sphene. The large-ion-lithophile elements, particularly Sr, Li, and Hf show some indication of depletion in the vein breccia relative to the host and the average MORB. Among the metallic elements, Ag, Cu, and Zn show marked enrichments of at least a factor of four relative to both the host basalt and MORB. Co and Pb show minor enrichments, and Cr, Ni and Sc are depleted in the hydrothermal breccia relative to the host basalt.

The other two breccias studied, RHGR-22 and RHGR-25, do not have a definitive relationship to a host rock. RHGR-22 is part of 23 cm radius sample of altered subrounded fragments of basalt with a matrix of clinochlore, saponite, and laumontite. RHGR-25 is composed of small subrounded fragments of basalt glass with alteration rims and a matrix of saponite, clinochlore and antigorite. Since the alteration mineralogy obscures any possible original matrix material the origin of this is uncertain. RHGR-25 in particular shows flow structures in the matrix that may have originated in volcanic glass, suggesting the brecciation may have been associated with a volcanic flow top rather than a hydrothermal system. The chemistry of these breccias is typical of the greenschist basalts described above.

Table 10. Microprobe results of silicate minerals in matrix of hydrothermal breccia RHGR-5

	Spot 1 Epidote	Spot 2 Epidote	Spot 3 Epidote	Spot 4 Sphene	Spot 5 pycnochlorite	Spot 6 pycnochlorite
SiO_2	36.20	35.48	36.16	31.32	28.61	27.64
TiO_2	.36	.32	1.32	35.46	.04	.04
Al_2O_3	24.36	23.06	22.38	5.01	27.13	28.01
FeO	13.01	13.03	13.40	3.96	25.11	24.44
MnO	.63	.67	.78	.08	.95	.83
MgO	.33	.32	.56	1.10	11.11	11.06
CaO	23.02	22.56	23.09	27.32	.31	.49
Na_2O	.03	.03	.04	.14	.15	.18
K_2O	.03	.02	.03	.16	.16	.20
Extra Oxygen	2.03	3.97	2.24	--	6.43	6.57

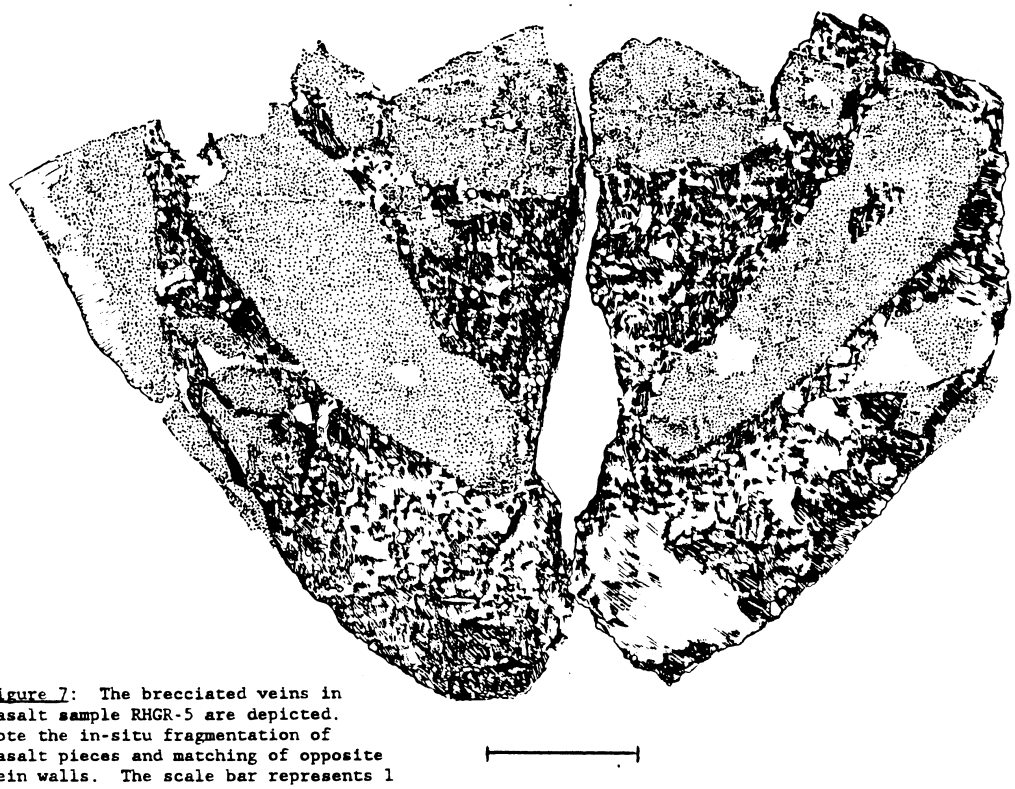

Figure 7: The brecciated veins in basalt sample RHGR-5 are depicted. Note the in-situ fragmentation of basalt pieces and matching of opposite vein walls. The scale bar represents 1 cm. Microprobe analysis of the silicates are given in table 10, and the sulfides in table 11.

Table 11. Microprobe Analysis of Sulphides in Hydrothermal Epidote-Chlorite vein Breccia (RHGR-5)

	Chalcopyrite	Chalcopyrite	Chalcopyrite	Chalcopyrite	Sphalerite	Sphalerite
S	35.30	35.63	35.54	35.04	31.08	31.68
Cu	33.66	32.93	32.63	33.06	2.13	3.24
Fe	30.28	30.04	30.84	30.93	6.03	4.03
Zn	.05	.10	.19	.10	60.13	59.41
Sb	.24	.18	.26	.19	--	--
As	.11	.10	.14	.13	--	--
Mn	.05	.06	.06	.07	--	--
Ni	.12	.13	.14	.13	.07	.06
Cr	.04	.05	.05	.07	.08	.09
	Sphalerite	Sphalerite	Sphalerite	Pyrite	Pyrite	Pyrite
S	34.07	33.68	33.53	54.28	54.31	54.29
Cu	1.21	2.23	1.18	.10	.10	.11
Fe	3.63	4.89	3.53	47.29	46.92	46.84
Zn	54.36	54.36	56.43	.08	.09	.08
Sb	--	--	--	.11	.13	.07
As	--	--	--	.07	.08	.14
Mn	--	--	--	.09	.10	.07
Ni	.11	.16	.17	.08	.09	.09
Cr	.03	.10	.12	--	--	--

Siliceous Samples

Because of the rarity of documented samples of hydrothermal quartz in the oceanic regime, the silica rich samples are given individual attention in this section. RHGR-6 consists of four fragments of quartz vein material (83% SiO_2) up to 2 cm in diameter. Inclusions of chlorite, albite, sphene, and basalt fragments are apparent and probably account for significant amounts of

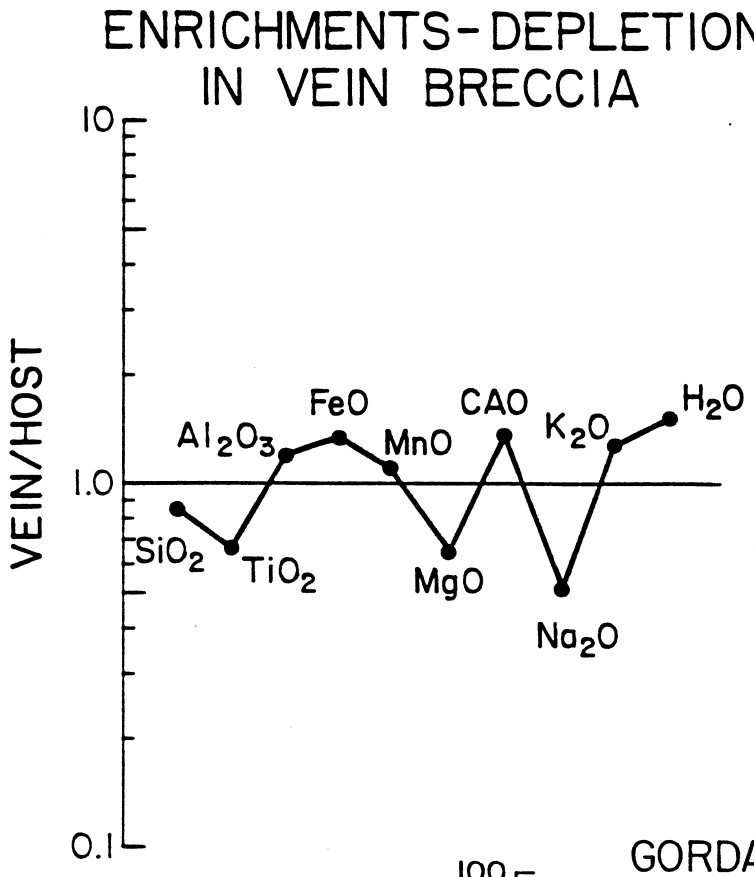

Figure 8: This figure depicts the enrichment and depletion factors of major elements in the brecciated hydrothermal vein of RHGR-5 compared to the host basalt.

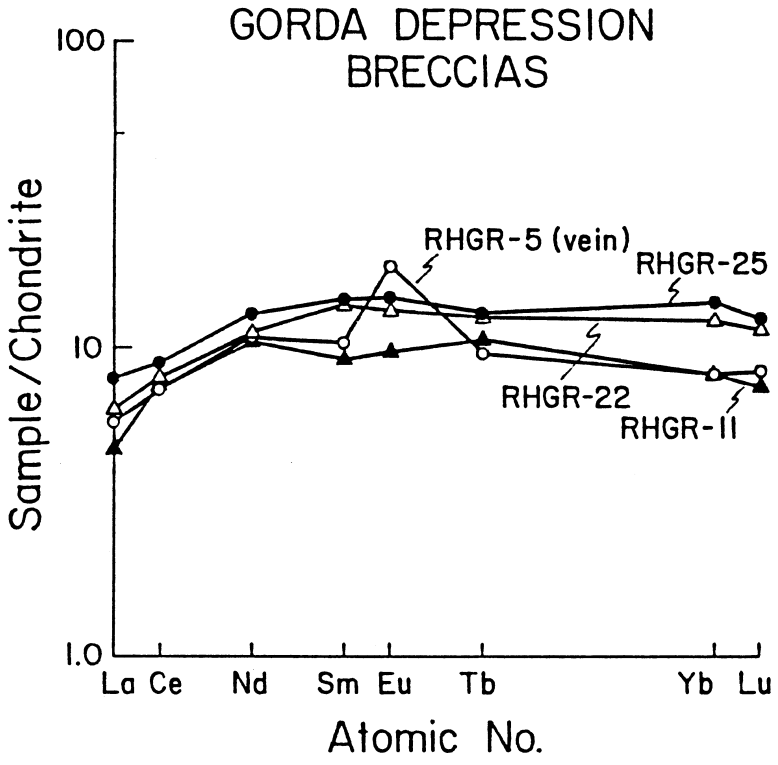

Figure 9: The REE patterns of Gorda Ridge breccias are shown. The patterns are similar to those expected for ocean ridge basalt with the exception of hydrothermal breccia vein in RHGR-5 which shows a clear positive Eu anomaly, perhaps because of the substitution of Eu for Ca in epidote.

Table 12. Composition of Sulphides from Quartz Veins (weight percent)

Mineral Type	Bornite	Bornite-Chalcopyrite	Chalcopyrite	Chalcopyrite	Chalcopyrite	Chalcopyrite	Chalcopyrite	Chalcopyrite
Sample No.	RHGR 6-0-6	RHGR 6-0-5	RHGR 6-0-5	RHGR 6-0	RHGR 6-2-2	RHGR 6-2-2-2	RHGR 6-2-2-3	RHGR 6-0-3
S	15.55	28.22	37.02	14.23	20.98	35.06	33.19	31.96
Cu	55.76	50.34	42.46	47.36	38.99	38.08	33.97	33.38
Fe	14.36	17.53	13.36	27.52	29.30	22.76	30.45	31.15
Zn	0.0	0.00	0.00	0.00	.96	.24	.33	0.00
Pb	0.0	0.00	0.00	0.00	0.00	0.00	0.00	0.00
Si	14.33	3.92	7.17	10.82	5.26	2.57	1.30	3.51
Al	-	-	-	-	4.21	1.27	.74	-
Cl	-	-	-	-	.19	0.00	0.00	-
Sb	0.0	0.0	0.0	0.0	0.0	0.00	0.00	0.00
As	0.0	0.0	0.0	0.0	.11	.02	0.03	-
Mn	-	-	-	-	-	0.00	-	-

Mineral Type	Sphalerite-Chalcopyrite	Chalcopyrite	Chalcopyrite	Chalcopyrite	Chalcopyrite	Chalcopyrite	Chalcopyrite	Galena
Sample No.	RHGR 6-2-1	RHGR 6-0-1	RHGR 6-2-3	RHGR 6-2-4	6-2-2-1	6-2-0	6-0-4	6-1-1 (Pb)
S	31.97	35.30	33.26	34.19	39.95	41.31	48.90	22.22
Cu	33.19	39.27	32.63	31.38	29.90	28.86	23.02	2.23
Fe	1.05	29.00	29.94	28.63	26.91	27.32	22.94	0.14
Zn	39.92	-	.59	0.20	0.38	0.43	-	1.72
Pb	0.00	-	.03	0.00	0.15	0.37	0.00	72.18
Si	.94	2.73	2.49	3.25	1.68	1.72	3.24	1.51
Al	0.00	-	1.05	2.30	1.04	0.00	0.00	-
Cl	0.00	-	0.00	0.00	0.00	0.00	0.00	0.00
Sb	0.00	0.00	0.00	0.00	0.00	0.00	0.00	-
As	-	0.00	0.00	0.05	0.00	0.00	-	-
Mn	0.00	-	-	0.00	-	0.00	-	0.00

Al_2O_3, Fe_2O_3 , MgO, and CaO in the analyses. The siliceous samples are enriched in Ag (.8 ppm), Cu (3610 ppm), and Zn (621 ppm) and to a lesser extent Li (24.5 ppm) and are depleted in Sr. The dominant sulfide is chalcopyrite with lesser amounts of bornite, sphalerite, and galena. The elemental composition of sulfides from the quartz vein material are given in table 12. The high concentrations of copper and visual inspection, suggests the quartz vein material contains 1 to 5% total sulfides.

In addition to quartz vein material, several 4cm diameter fragments of hydrothermal breccia cemented by cryptocrystalline quartz were analyzed (RHGR-11). Subrounded fragments of phyric greenstone basalt and to a lesser extent carbonate and mafic tectonite comprise 50 to 70% of the rock. The brecciated fragments range from sub-millimeter to 5 mm in diameter. The matrix is cryptocrystalline quartz showing at least two stages of fragmentation and silica precipitation with the last stage represented by coarser grained nearly pure quartz. The main features of the silicified breccia are shown in Fig. 10 and pertinent microprobe data given in table 13.

A characteristic feature of the silicified breccia is the evidence for multiple in-situ fragmentation events. As shown in Fig. 10, basalt fragments are shattered in place, cemented in place, and then shattered by another fragmentation event. Furthermore, the borders of basalt fragments show partially dissolved pieces cemented together by cryptocrystalline quartz. These features can be best explained by concurrent brecciation and solution-deposition in hydrothermal systems as described from breccias on the Mid-Atlantic Ridge by Delaney et al (1986). Amorphous hydrothermal silica has also been described associated with sulfide deposition in the basement basalts of DSDP site 471 (Devine and Leinen 1981), interlayer vugs in sulfide chimneys from the east Pacific Rise (Hekinian et al., 1980; Bischoff et al., 1983) and more recently as the main constituent of hotspring vent chimneys on

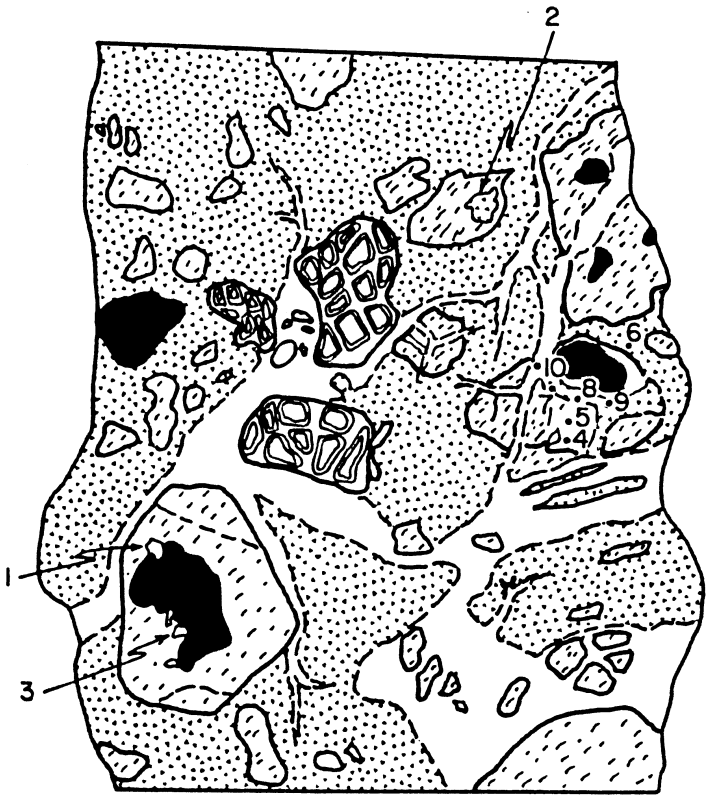

Figure 10: A Diagrammatic representation of silicified breccia RHGR-11 showing pyrite inclusions (black area) in fragments of chlorite-albite rich basalts (dashed areas). Fragments of mafic tectonite (see Fig. 3) are represented by areas with colloform style banding. The area with triangles represents the first stage silicified matrix with 20 to 50% sub mm size fragments of basalts. A later stage fracturing and silicification cuts across this earlier silicified matrix and is represented by the clear areas. Microprobe spots given in table 13 are indicated by the numerals. Note the basalt fragments in the right center. Two fragments of basalt have been shattered and cemented together by the silica matrix. The lower of the two fragments was shattered twice by subsequent invasions of silica bearing solutions. Scale bar represents 1 cm.

Table 13. Microprobe Results
for silicate phases in hydrothermal siliceous breccias
(see Fig. 10 for spot locations)

	Spot 1 albite in basalt fragment	Spot 2 albite in basalt fragment	Spot 3 albite in basalt fragment	Spot 4 altered glass in basalt fragment	Spot 5 altered glass in basalt fragment
SiO_2	68.49	67.10	65.17	31.24	50.43
TiO_2	.04	.04	.04	.15	.04
Al_2O_3	19.45	18.45	20.25	21.00	25.42
FeO	.06	.22	.16	13.20	.59
Mn	.05	.05	.06	.50	.04
MgO	.06	.06	1.58	1.01	.42
CaO	.21	.09	10.82	16.95	1.02
Na_2O	11.38	11.69	.19	.47	6.75
K_2O	.09	.06	1.70	.35	.14
Extra Oxygen	.19	2.24		15.15	15.14

	Spot 6 Clinochlore in breccia matrix	Spot 7 Clinochlore in breccia matrix	Spot 8 First stage silicified zone	Spot 9 first stage silicified zone	Spot 10 last stage silicification
SiO_2	29.83	30.92	88.53	84.29	96.05
TiO_2	.04	.04	2.71	.04	.04
Al_2O_3	15.95	24.69	2.23	4.50	.97
FeO	19.86	18.01	.60	3.08	.20
Mn	.34	.32	.04	.07	.04
MgO	21.03	17.05	.25	2.37	.04
CaO	.08	.42	.24	.21	.05
Na_2O	.20	.10	.08	.10	.05
K_2O	.13	.13	.16	.14	.05
Extra Oxygen	12.47	8.32	5.15	5.21	2.46

the Galapagos Rise and Juan de Fuca Ridges (Embley 1986, personal communication). The association of silica rich zones with massive sulfides and gold deposition in ophiolites is well documented, but unlike the silicification processes in Archaean ophiolites (deWit et al. 1982), these samples do not show pervasive replacement of the fragments by silica. Furthermore, although the samples contain abundant pyrite, it is mainly hosted in the basalt fragments rather than in the silica matrix suggesting, unlike the quartz vein material described above, that the pyrite deposition was not synchronous with silicification.

DISCUSSION: ELEMENT MOBILITY AND METALLOGENESIS IN THE GORDA DEPRESSION HYDROTHERMAL SYSTEM.

The studies described in the previous section allow some conjecture on the parameters of the hydrothermal system which acted on the samples dredged from the Gorda Depression. Of particular interest are depth, temperature, and water/rock ratio. The data suggest a complex system in which veins and brecciated zones underwent multiple stages of fracturing and precipitation of hydrothermal phases. Late stage events overprinted earlier formed assemblages. This complex relationship of changing conditions is characteristic of hydrothermal stockwork zones described on the Mid-Atlantic ridge and Costa Rica Rift (Delaney et al., 1986; Honnorez et al., 1985).

A schematic representation of the mineralogical stratigraphy imposed on the oceanic crust by seawater interaction is shown in Fig. 11 where it is compared to the results on the Gorda Depression samples. Typically,

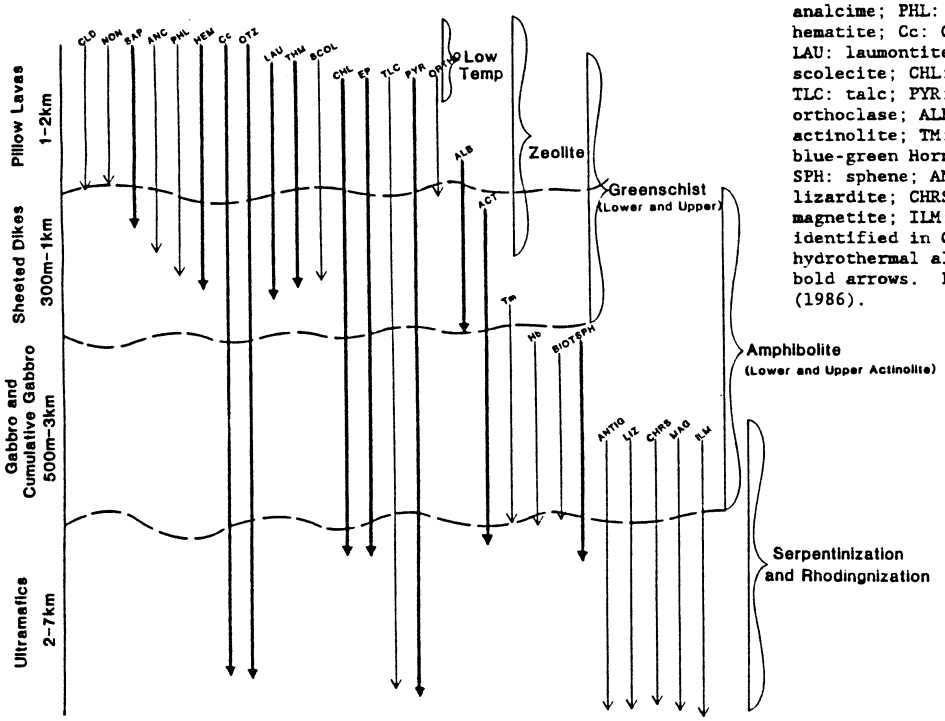

Figure 11: Schematic representation of the relationship between metamorphic mineral zoning and depth in the oceanic crust. CLD: celadonite; NON: nontronite; SAP: saponite; ANC: analcime; PHL: phillipsite; HEM: hematite; Cc: Calcite; QTZ: quartz; LAU: laumontite; THM: thomsonite; SCOL: scolecite; CHL: chlorite; EP: epidote; TLC: talc; PYR: pyrite; ORTHO: orthoclase; ALB: albite; ACT: actinolite; TM: tremolite; Hb: blue-green Hornblende; BIOT: biotite; SPH: sphene; ANTIG: antigorite; LIZ: lizardite; CHRS: chrysotile; MAG: magnetite; ILM: ilmenite. The minerals identified in Gorda Depression hydrothermal alteration are depicted by bold arrows. From deWit et al., (1986).

analcite, chlorite, quartz, saponite, and epidote occurs in the upper sheeted dikes and pillow lava sections. Albite and actinolite are normally thought to be diagnostic of the sheeted dikes and upper massive gabbro zone. The Gorda Depression dredge hauls contain gabbro altered to actinolite and albite suggesting formation and alteration at a minimum BSF (Below Sea Floor) depth of 1300m. On the other hand, the glassy basalts with saponite, chlorite, and analcite could have formed very near to the top of the volcanic crust.

The effective water/rock ratio plays a role in determining hydrothermal stability fields within the oceanic crust. In the case of seawater, high water/rock ratios promote stability of Mg-rich phases such as chlorite and the serpentine minerals (Reed 1982). This observation suggests that at 350°C bands or halos of mineral assemblages are expected with chlorite-serpentine minerals forming on the outside of basalt fragments or in the center of fissures and faults where seawater access is high, whereas albite-actinolite would form in low water/rock zones such as the interior of basalt fragments or in the wall rock zones of faults and fissures. This observation may explain the banding in RHGR-21 (Fig. 3).

The solubility of various chemical species in hydrothermal solution is strongly temperature dependant. In particular Mg displays a retrograde solubility forming insoluble Mg(OH) complexes at high temperatures. On the other hand, as shown in Fig. 12, the solubility of SiO_2 increases in hydrothermal solutions with temperature. The net results is a well documented inverse relationship between MgO and SiO_2 in hydrothermally altered volcanic rocks. The Gorda Depression samples suggest in Fig. 13 a relationship between MgO and SiO_2 as expected by hydrothermal metamorphism over variable temperatures from 120°C to 400°C. Unlike MgO and SiO_2, CaO has a solubility minimum in a limited temperature range and re-dissolves at both lower and higher temperatures. The kinetics of reaction at low temperatures probably prohibit significant re-solution of Ca.

The life cycle of hydrothermal solutions and associated mineralization can best be understood by dividing it into two stages.

1) The heating, reduction, and acidification of seawater as it enters the oceanic crust

2) The cooling and oxidation of mature mineral laden solutions as they exit the crust.

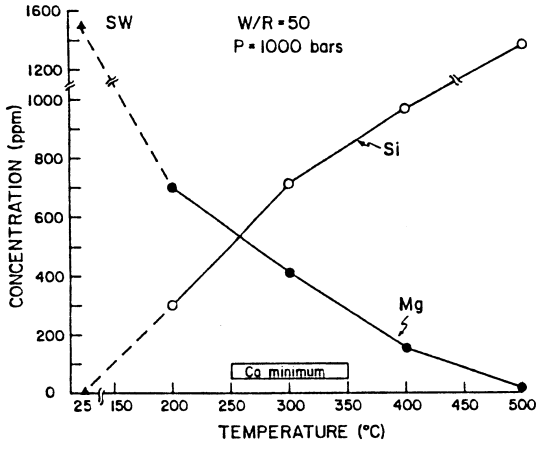

Figure 12: The solubility of Mg and Si in hydrothermal fluids in basalt/seawater experiments. The box labeled Ca minimum represents the range of minimum solubility of Ca in hydrothermal solutions in the temperature range of 250 to 350°C. Data from Chandler and Hajash (1985).

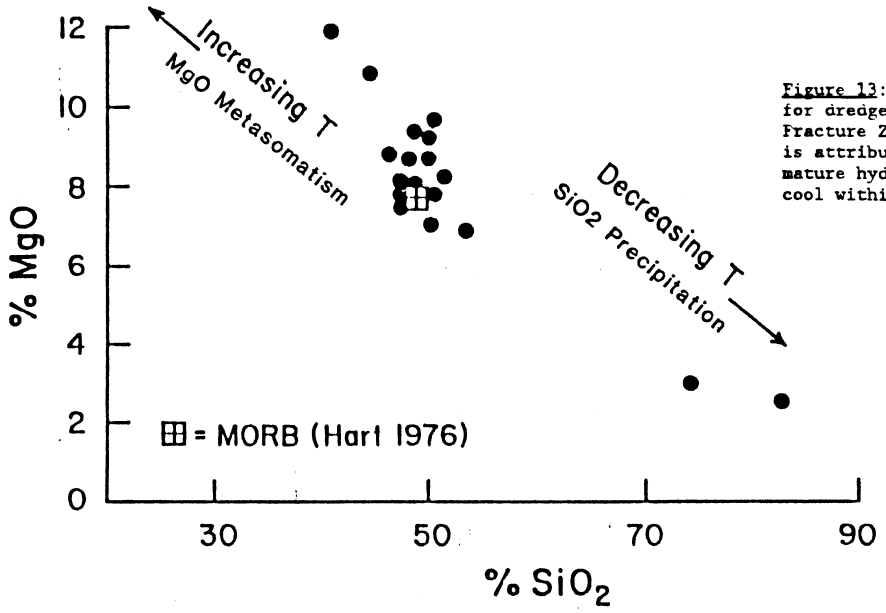

Figure 13: A plot of %MgO vs. $\%SiO_2$ for dredge samples from the Blanco Fracture Zone. The enrichment of SiO_2 is attributed to silicification by mature hydrothermal solutions as they cool within the oceanic crust.

Seawater as it enters the oceanic crust carries excess Mg, Na, SO_4, O_2, Cr, Ni and perhaps platinoids and Au. Because of the process of hydrolysis of H_2O in forming Mg(OH) groups, the solution becomes acidic and reducing. The metals Fe, Cu, Zn, Pb, Co, and Ag are leached from the volcanic rocks along with SiO_2 and Ca (at temperatures above 350°C). The mineralogy of the Gorda Depression greenschist gabbros are consistent with formation at this stage of hydrothermal activity. The depletion of Cu and Zn and enrichment of Cr and Ni in the gabbros relative to MORB (Fig. 14) are especially diagnostic of formation in immature hydrothermal solutions at high temperature. The increase of Cr with MgO in the Gorda Depression samples (Fig. 15) suggests Cr is stripped from seawater along with Mg in the Blanco Fault Zone.

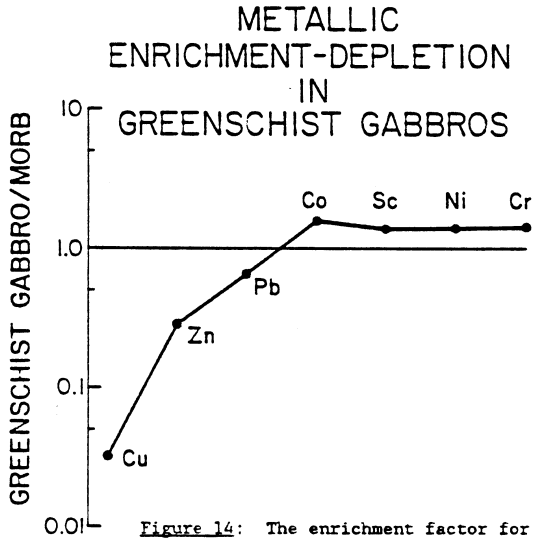

Figure 14: The enrichment factor for the metallic elements in Gorda Depression Greenschist Gabbros.

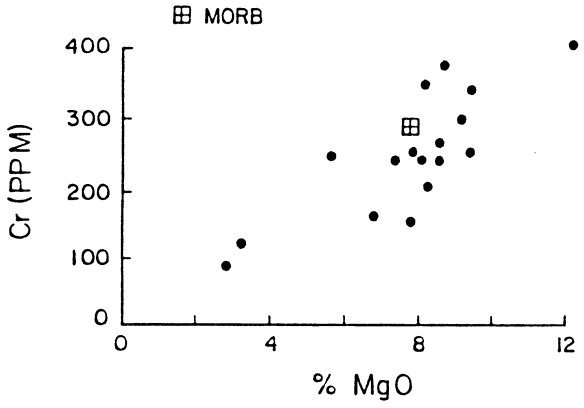

Figure 15: A plot of Cr vs. %MgO is shown for all Gorda Depression samples.

The second stage in the life cycle of hydrothermal solutions is the precipitation of authigenic hydrothermal phases from the solutions as they cool. At least two types of authigenic mineralization are represented in the Gorda Ridge samples. The first might be appropriately called Al and Fe metasomatism because of the deposition of chlorite and epidote in the groundmass, cavities, and veins of basalts and breccias. This stage, as shown in Fig. 16, is characterized by enrichments of Ag, Cu, Zn, Pb, and Co, and depletion of Sc, Cr, and Ni. The last phase of the cooling mature hydrothermal solutions precipitates silica to form siliceous breccias that contain fragments of the earlier formed chlorite rich samples. The quartz vein material is highly enriched in Ag, Cu, and Zn and depleted in Cr (Fig. 17). Thus, the samples yield a consistent pattern of deposition of Cr, Ni, and Sc at high temperatures from immature solutions with leaching of Ag, Cu, Zn, Pb and Co, and just the opposite at low temperature. The sulfides minerals pentlandite and pyrrhotite probably precipitated from evolved seawater entering the fault zone and sphalerite, chalcopyrite, bornite, sphalerite, and galena formed at low temperatures by exiting mature solutions. The association of sulfide mineral type and host rock is shown in Fig. 18.

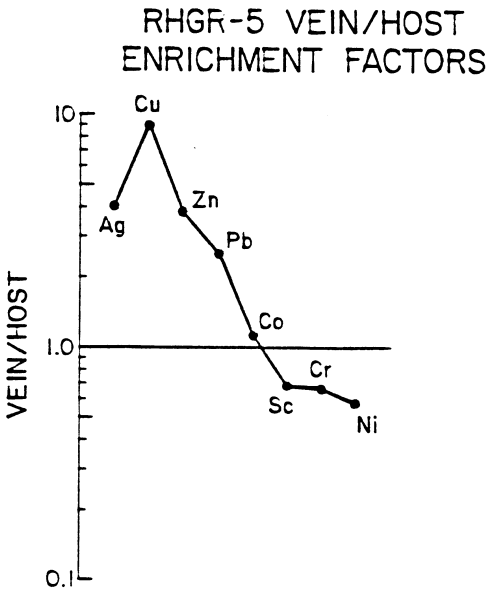

Figure 16: The enrichment factors for metallic elements in the brecciated hydrothermal vein (RHGR-5) compared to the host rock. The matrix of the vein is chlorite and epidote.

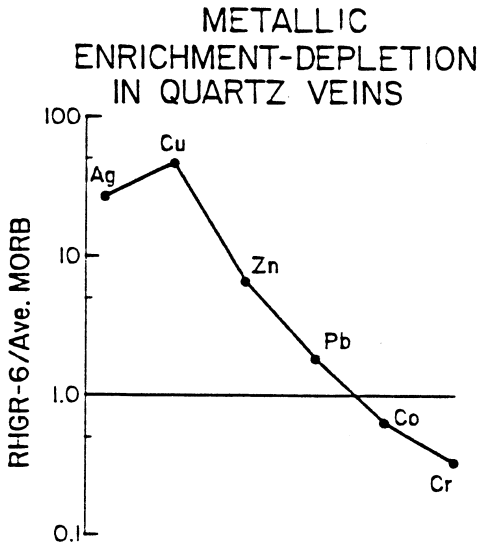

Figure 17: The metallic element enrichment factors in quartz veins (RHGR-6) compared to MORB.

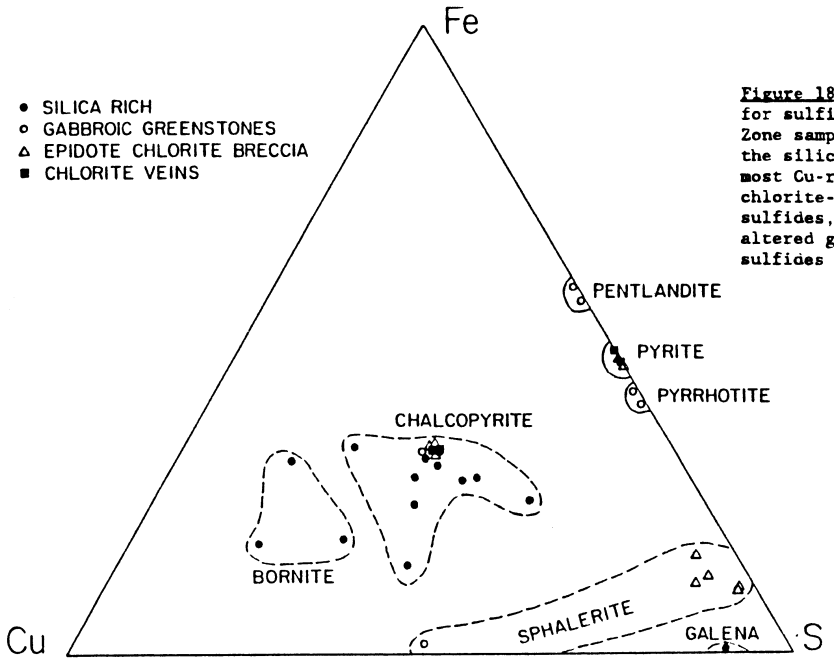

Figure 18: A tri-plot of Cu, Fe, and S for sulfide minerals in Blanco Fracture Zone samples. The plot indicates that the silica-rich host rocks have the most Cu-rich sulfides, that the chlorite-epidote veins contain Zn-rich sulfides, and that the high-temperature altered gabbros contain Ni-rich sulfides (pentlandite).

CONCLUSIONS

1) Hydrothermally altered basalts, gabbros and breccias from the Gorda Depression were metamorphosed in multiple stages representing temperatures from 120°C to upwards of 400°C. Formation of saponite and analcite in glassy basalts at low temperature was followed by vein filling of laumontite then chlorite. Actinolite, representing the highest temperature, formed concurrently with chlorite in some cases. Some of the samples were then brecciated and cemented with crypotocrystalline quartz as the mature hydrothermal solutions cooled.

2) Although some features of the brecciation may be volcanogenic or tectonic, evidence of hydrothermal brecciation is in abundance. This includes fragmentation of sulfide minerals as they precipitated, multiple fragmentation events with latter events fracturing earlier formed matrix cements, rounding of basalt fragments in breccias by fluid attrition and preservation of matching vein and fragment edges.

3) Sulfide mineralization occurred in at least three distinct phases, perhaps representing different stages in the evolution of seawater into mature hydrothermal solution and then cooling of these solutions as they exited from the oceanic crust. Evidence suggest Mg, Cr, and Ni are stripped from seawater during heating of seawater in exchange for Si, Cu, Zn, and Pb in the gabbroic portions of the crust in the Blanco Fracture Zone. Chlorite and epidote veins enriched in Al and Fe were formed during cooling of mature solutions with synchronous formation of chalcopyrite, sphalerite, and pyrite. As the solutions cooled further, silicification and brecciation resulted with precipitation of bornite, chalcopyrite, sphalerite, galena, and pyrite.

ACKNOWLEDGMENTS

This work was funded by the Gorda Ridge Task Force through a grant to Oregon State University by the Oregon Department of Geology and Mineral Industries. The authors are grateful to the USGS Marine Geology Branch for both space and ship time on the R/V Lee and the officers, crew, scientists and technicians for their able support. The dredging was carried out under supervision of Dr. David Clague and Mr. Andrew Stevenson.

SCEM analysis were provided by Drs. George Dooley and Charles Dellenbach of the U.S. Bureau of Mines. We are grateful to Greg Campi, Bobbi Conard and Sandy Moore of OSU Oceanography for analytical capabilities; to Dave Wendland for thin section investigation and Michael Schaeffer of U. of O. for guidance in use of the microprobe.

The authors benefited from many useful discussions with Drs. Robert Dill, Greg McMurray, John Smith, Don Hull, Martin Fisk and Jack Dymond. The manuscript was greatly improved as a result of critical readings by Joseph Ritchey, David Clague, and Robert Duncan.

REFERENCES

Alt, J.C., Laverne, C., and Muehlenbachs. 1985. Alteration of the upper oceanic crust: Mineralogy and processes in Deep Sea Drilling Project Hole 504B, Leg 83. In, Anderson, R.N., Honnorez, J., Becher, K. et al, Initial Reports of the Deep Sea Drilling Project, v. 83. Washington, D.C. (U.S. Govt. Printing Office).

Bass, M.N., Moberly, R., Rhodes, J.M., Shih, C.S., Church, S.E. 1973. Volcanic rocks cored in the central Pacific leg 17 Deep Sea Drilling Project. Initial Reports of Deep Sea Drilling Project, v. 17:429-503. Washington, D.C. (U.S. Govt. Printing Office).

Beaty, D.W., and Taylor, H.P., Jr. 1980. Early crustal hydrothermal processes and the $^{18}O/^{16}O$ evolution of seawater; evidence form the Amulet mine, Quebec [abs.]. EOS, v. 61, No. 17:386.

Bischoff, J.M., Aruscavage, P.J., Baedecher, P.A., and Crock, J.G. 1983. Geochemistry and economic potential of massive sulfide deposits from the Eastern Pacific Ocean. USGS open-file report 83-324.

Bonatti, E., Guerstein-Honnorez, B.M., and Honnorez, J. 1976. Copper-iron sulfide mineralizations from the equatorial Mid-Atlantic Ridge. Econ. Geol., 71:1515-1525.

Cann, J. 1980. Availability of Sulphide Ores in the Oceanic Crust. J. Geol. Soc. London, v. 137:381-384.

Cocker, J.D., Griffin, B.J., Muehlenbachs, K. 1982. Oxygen and carbon isotope evidence for seawater-hydrothermal alteration of the Mcquarie Island ophiolite. Earth Planet. Sci. Lett., 61:112-122.

Coish, R.A. 1977. Ocean floor metamorphism in the Betts Cove ophiolite, Newfoundland. Contrib. Mineral. Petrol., 60:255-270.

Coleman, R.G., Huston, C., El-Boushi, I.M., Al-Hinai, K.M., and Bailey, E.H. 1978. Occurrence of copper-bearing massive sulphides in the Semail ophiolite, Sultanate of Oman: Precambrian Research, v. 6:A11-A12.

Constantinou, G. 1980. Metallogenesis associated with the Troodos ophiolite. in Panayioutou, A., ed. Ophiolites: Internat. Ophiolite Symposium, Cyprus, 1979, Proc.: Cyprus, Ministry Agriculture Nat. Resources, Geol. Survey Dept., 663-674.

Corliss, J.B., Dymond, J., Gordon, L.I., Edmond, J.M., von Herzen, R.P., Ballard, R.D., Green, K., Williams, D., Bainbridge, A., Crane, K., van Andel, T.H. 1979. Submarine thermal springs on the Galapagos Rift. Science, 203:1073-1083.

Crane, K. 1976. The intersection of the Siqueiros Transform Fault and the East Pacific Rise. Marine Geol., 21:25-46.

de Beer, J.H., Stettler, E.H., Barton, J.M., Jr., van Reenen, D.D., and Vearncombe, J.R. 1986. Crustal Structure of the Archean Granite-Greenstone Terrane in the Northern Portion of the Kaapvaal Craton.

Lunar and Planetary Institute Workshop on Tectonic Evolution of Greenstone Belts, Houston, Texas, 23-24.

Delaney, J.R., Moyk, D.W., and Mottle, M.J. 1986. Quartz-cemented, Sulfide-Bearing Greenstone Breccias From the Mid-Atlantic Ridge -Samples of a High-Temperature Hydrothermal Upflow Zone. Science, in press.

Devine, Joseph D. and Leinen, Margaret. 1981. Chemistry of the Massive Sulfide Deposit Cored at Site 471. In Yeats, R.S., Hog. B.U., et al. Initial Reports. DSDP 63:679-682. Washington, D.C. (U.S. Govt Printing Office).

deWit, M.J., Stern, C.R. 1976. Ocean floor metamorphism, seismic layering and magnetism. Nature, 264:615-619.

deWit, M.J., Hart, R.A., Marten, A., Abbott, P. 1982. Archean abiogenic and probable biogenic structures associated with mineralized hydrothermal vent systems and regional metasomatism with implications for Greenstone Belt studies. Econ. Geol., 77:001.

deWit, M.J., Hart, R, and Hart, R. 1986a. A Mid-Archean Ophiolite Complex, Barberton Mountain Land. Lunar and Planetary Institute Workshop on the Tectonic Evolution of Greenstone Belts, Houston, Texas, 27-29.

Donnelly, T.W., Thompson, G., Robinson, P.T. 1979. Very low temperature hydrothermal alteration of the oceanic crust and the problem of fluxes of potassium and magnesium. In Deep Drilling Res.: Ocean Crust. ed. M. Talwani, C.G.A. Harrison, D.E. Hayes, 2nd Maurice Ewing Symposium, v. 369-392. Washington, D.C., Amer. Geophys. Union.

Edmond, J.M., Measures, C., Mangun, B., Grant, F.R., Sclater, F.R., Collier, R., Hudson, A., Gordon, L.I., Corliss, J.B. 1979a. On the formation of metal-rich deposits at ridge crests. Earth Planet. Sci. Lett., 46:19-30.

Edmond, J., Measures, R.E., McDuff, R.E., Chen, L.H., Collier, R., Grant, B., Gordon, L.I., Corliss, J.B. 1979b. Ridge crest hydrothermal activity and the balances of the major and mionor elements in the ocean: The Galapagos data. Earth Planet. Sci. Lett., 46:1-18.

Elthon, D. 1981. Metamorphism in oceanic spreading centers. In Emiliani, C. ed., The Sea, v. 7, John Wiley & Sons, NY, 285-303.

Elthon, D., Lawrence, J.R., Hanson, R.E., Stern, C. 1984. Modeling of oxygen isotope data from the Sarmiento Ophiolite Complex, Chile, with implications for ocean floor metamorphisms. J. Geol. Soc. London, in press.

Ferrario, A., and Garuti, G. 1980. Copper deposits in the basal breccias and volcano-sedimentary sequences of the eastern Ligurian ophiolites (Italy). Mineralium Deposita, v. 15:291-303.

Francheteau, J., Needham, H., Choukroune, P., Juteau, T., Seguret, B., Ballard, R.D., Fox, P., Mormark, W., Carranza, A., Cordoba, D., Guerrero, J., Rangin, C., Bougault, H., Cambon, P., and Hekinian, R.

1979. Massive Deep-Sea Sulphide Ore Deposits Discovered on the East Pacific Rise. Nature, v. 277:523-528.

Franklin, J.M., Lydon, J.W. and Sangster, D.F. 1981. Volcanic-Associated Massive Sulfide Deposits. Economic Geology 75th Anniversary Volume. 485-627.

Fripp, R.E.P. 1986. The Yilgarn Craton Western Australia: a Tectonic Synthesis: 1. Lunar and Planetary Institute Workshop on the Tectonic Evolution of Grenstone Belts, Houston, Texas, 39-40.

Fyfe, W.S., and Lonsdale, P. 1981. Ocean Floor Hydrothermal Activity. In Emiliani, C. ed., The Sea, v. 7, John Wiley & Sons, NY

Gregory, R.J., Taylor, H.P. 1981. An oxygen isotope profile in a section of cretaceous oceanic crust: Samail Ophiolite, Oman: Evidence of $\delta^{18}O$ buffering of the oceans by deep (>5 km) seawater-hydrothermal circulation at mid-ocean ridges. J. Geophys. Res., 86:2737-2755.

Harper, G.D. 1986. Dismembered Archean Ophiolite in the Southeastern Wind River Mountains, Wyoming -- Remains of Archean Oceanic Crust. Lunar and Planetary Institute Workshop, Houston, Texas, 47-49.

Hart, R.A. 1970. Chemical exchange between sea water and deep ocean basalts. Earth Planet Sci. Lett., 9:269.

Hart, R.A. 1973a. A model for the chemical exchange in the basalt-seawater system of oceanic layer 2. Can. J. Earth Sci., 10:799-816.

Hart, R.A. 1973b. Geochemical and geophysical implications of the reaction between sea water and the oceanic crust. Nature, 243:76-78.

Hart, S.R., Erlank, A.J., Kable, E.S.D. 1974. Sea floor alterations: Some chemical and Sr isotopic effects. Contr. Mineral. Petrol., 44:219-230.

Hart, S.R., Staudigel, H. 1982. The control of alkalics and uranium in seawater by ocean crust alteration. Earth Planet. Sci. Lett., 58:202-212.

Heirtzer, J.R. 1972. Understanding the Mid-Atlantic Ridge. Natl. Acad. Science, 131pp. Washington, D.C.

Hekinian, R., Fevrier, M., Bischoff, J., Picot, P., and Shanks, W. 1980. Sulfide deposits from the East Pacific Rise near 21°N: A mineralogical and geochemical study. Science, v. 207:1422-1444.

Helmstaedt, and Padgham, W.A. 1986. Evidence for Spreading in the Lower Kam Group of the Yellowknife Greenstone Belt: Implications for Archean Basin Evolution in the Slave Province. Lunar and Planetary Institute Workshop on the Tectonic Evolution of Greenstone Belts, Houston, Texas, 55-58.

Hoffert, M., Perseil, A., Hekinian, R., Chouberoune, P., Needham, H.D., Francheteau, J., and LePechon X. 1978. Hydrothermal deposits sampled by diving saucer in Transform "A" near 37°N on the Mid-Atlantic, Famous

Area. Oceanol. Acta., 1:72-86.

Honnorez, J., Alt, J.C., Honnorez-Guertsein, B.M., Laverne, C., Muehlenbachs, K., Duiz, J., and Saltzman, E. 1985. Stockwork-like sulfide mineralization in young oceanic crust: Deep Sea Drilling Project Hole 504B. In Anderson, R.N., Honnorez, J., Becher, K. et al., Initial Reports of the Deep Sea Drilling Project, v. 83. Washington (U.S. Govt. Printing Office)

Humphris, S.E., Thompson, G. 1978a. Hydrothermal alteration of oceanic basalts by seawater. Geochim. Cosmochim. Acta, 42:107.

Humphris, S.E., Thompson, G. 1978b. Trace element mobility during hydrothermal alteration of oceanic basalts. Geochim. Cosmochim. Acta, 42:127-136.

Hunter, D.R., Wilson, A.H., Versfeld, J.A., Allen, A.R., Smith, R.G., Sleigh, D.W.W., Groenewald, P.B., Chutter, G.M., and Preston, V.A. 1986. A Continuous Record of Tectonic Ecolution from 3.5 Ga to 2.6 Ga in Swaziland and Northern Natal. Lunar and Planetary Institute Workshop on Tectonic Evolution of Greenstone Belts, Houston, Texas, 64-68.

Jankovic, S. 1980. Porphyry-copper and massive-sulfide ore deposits in the northeastern Mediterranean. in Ridge, J.D., ed. IAGOD Symposium, 5th, Proc: Stuttgart, E. Schweizerbart'sche Verlagsbuchhandlung, 431-444.

Jenkins, W.J., and Clarke, W.B. 1976. The distribution of ^{3}He in the western Atlantic Ocean. Deep-Sea Res., 23:481-494.

Juteau, T., Noack, Y., Whitechurch, H., Courtois, C. 1979. Mineralogy and geochemistry of alteration products in holes 417A and 417D basement samples (Deep Sea Drilling Project). In Initial Reports of Deep Sea Drilling Project. vol. 53. ed. T. Donnelly, J. Franchetau et al., 1273-1279. Washington, D.C. (U.S. Govt. Printing Office).

Koski, R.A., and Derkey, R.E. 1981. Massive Sulfide deposits in oceanic-crust and Island-arc terranes of southwestern Oregon. Oregon Geology, v. 43, No. 9:119-125.

Koski, R.A., Normark, W.R., Morton, J.L., and Delaney J.R. 1982. Metal Sulfide Deposits on the Juan de Fuca Ridge. Oceanus, 253:42-48.

Koski, R.A., Goodfellow, R., and Bouse, R.M. 1982. Preliminary description of massive sulfide samples from the southern Juan de Fuca Ridge. U.S. Geological Survey Open-File Report 82-200B, 11.

Koski, R.A., Lonsdale, P.F., Shanks, W.C., Berndt, M.E., and Howe, S.S. 1985a. Mineralogy and Geochemistry of a Sediment-Hosted Hydrothermal Sulfide Deposits From the Southern Trough of Guayma Basin, Gulf of California. J.G.R., 90:6095-6707.

Koski, R.A., Clague, D.A., and Oridin. 1985b. Mineralogy and Chemistry of Massive Sulfide Deposits from the Juan de Fuca Ridge. Geological Society of America Bulletin, 95:930-945.

Lalou, C., Brichet, E., Ku, T.L., and Jehanno, C. 1977. Radiochemical, scanning electron microscope (SEM) and x-ray dispersive energy (EDAX) studies of a FAMOUS hydrothermal deposit. Marine Geol., 24:245-258.

Liou, J.G., Ernst, W.G. 1979. Oceanic ridge metamorphism of the east Taiwan ophiolite. Contrib. Mineral. Petrol., 68:335-348B.

Lonsdale, P.F., Bischoff, J.L., Burns, V.M., Kastner, M., and Sweeney, R.E. 1980. A high temperature hydrothermal deposit on the sea bed at a Gulf of California Spreading Center. Earth Planet. Sci. Lett., v. 49:8-20.

MacGeehan, P.J., and MacLean, W.H. 1980. An Archean sub-seafloor geothermal system, "calc-alkali" trends, and massive sulphide genesis. Nature, v. 286:767-771.

Malahoff, A. 1981. Comparison between Galapagos and Gorda Spreading Centers. 13th Ann. Offshore Tech. Conf., No. 4129, May 1981. 115-121.

Malahoff, A. 1982. A comparison of the massive submarine polymetallic sulfides of the Galapagos Rift with some continental deposits. Marine Technology Society Journal, v. 16, No. 3:39-45.

Martyn, J.E. 1986. Evidence for Structural Stacking and Repetition in the Greenstones of the Kalgoorlie District, Western Australia. Lunar and Planetary Institute Workshop, Houston, Texas, 75-77.

Normark, W.R., Lupton, J.E., Murray, J.W., Koski, R.A., Clague, D.A., Morton, J.L., Delaney, J.R., and Johnson, H.P. 1982. Polymetallic sulfide deposits and water column tracers of active hydrothermal vents on the southern Juan de Fuca Ridge. Marine Technology Society Journal, v. 16, No. 3:46-53.

Reed, M. 1983. Seawater-basalt reaction and the origin of greenstones and related ore deposits. Economic Geol. 78:80-90.

Roberts, R.G., and Reardon, E.J. 1978. Alteration and ore-forming processes at Mattagami Lake mine, Quebec. Can. Jour. Earth Sci., v. 15:1-21.

Rona, P.A. 1976. Pattern of hydrothermal mineral deposition: Mid-Atlantic Ridge Crest at Latitude 26°N. Marine Geol. 21, 59-66.

Sangster, D.F. 1980a. A review of Appalachian stratabound sulphide deposits in Canada. Ireland Geol. Survey, Spec. Paper, 5:7-18.

Selk, B.W. 1977. The Manganese-Enriched Sediments of the Blanco Trough: Evidence for Hydrothermal Activity in a Fracture Zone. M. Sc. Thesis, Oregon State University.

Seyfried, W.E., Mottl, M.J., Bischoff. 1978. Seawater/basalt/ratio effects on the chemistry and mineralogy of spilites from the ocean floor. Nature, 275:211-213.

Spiess, F.N., MacDonald, K.,m Atwater, T., Ballard, R., Carranza, A., Cordoba, D., Cox, C., Diaz Garcia, B., Francheteau, J., Guerrero, J., Hawkins, J., MacDougall, J.D., Miller, S., Normark, W., Orcutt, J., and Rangin, C. 1980. East Pacific Rise: Hot springs and geophysical

experiments. Science, v. 207:1421-1432.

Spooner, E.T.C. and Fyfe, W.S. 1973. Sub-seafloor metamorphism, heat and mass transfer. Contrib. Mineral. Petrol., 42:287-304.

Spooner, E.T.C., Chapman, H.J., and Sinewing, J.D. 1977. Strontium isotopic contamination and oxidation during ocean floor hydrothermal metamorphism of the ophiolite rocks of the Trodoos Massif, Cyprus. Geochim. cosmochim. Acta 41:873-890.

Stakes, D.S., and O'Neil, J.R. 1982. Mineralogy and stable isotope geochemistry of hydrothermally altered oceanic rocks. Earth Planet. Sci. Lett., 57:285-304.

Stern, C., and Elthon, D. 1979. Vertical variations in the effects of hydrothermal metamorphism in Chilean ophiolites: Their implications for ocean floor metamorphism. Tectonophysices, 55:179-213.

Thompson, G. 1973. A geochemical study of the low-temperature interaction of seawater and oceanic igneous rocks. DSDP Conference on Igneous and Metamorphic Rocks. EOS, Trans. Amer. Geophys. Union, 54:1015-1019.

Vidal, V.M., Vidal, F.V., and Isaacs, J.D. 1978. Coastal submarine hydrothermal activity off northern Baja California. J. Geophys. Res., 83:175-1774.

VonDamm, K.L., Edmond, J.M, Measures, C.I., and Grant, B. 1985. Chemistry of submarine hydrothermal solutions at Guayma Basin, Gulf of California. Geochimica et Cosmochemica Acta, 99:2227-2237.

Wolery, T.J., and Sleep, N.H. 1976. Hydrothermal circulation and geochemical flux at mid-ocean ridges. J. Geol., 84: 249-275.